

Interstellar Silicon Depletion and the Ultraviolet Extinction

DRAFT: 2018.9.28.711

Ajay Mishra^{1,2} and Aigen Li¹

ABSTRACT

Spinning small silicate grains were recently invoked to account for the Galactic foreground anomalous microwave emission. These grains, if present, will absorb starlight in the far ultraviolet (UV). There is also renewed interest in attributing the enigmatic 2175 Å interstellar extinction bump to small silicates. To probe the role of silicon in the UV extinction, we explore the relations between the amount of silicon required to be locked up in silicates $[\text{Si}/\text{H}]_{\text{dust}}$ and the 2175 Å bump or the far-UV extinction rise, based on an analysis of the extinction curves along 46 Galactic sightlines for which the gas-phase silicon abundance $[\text{Si}/\text{H}]_{\text{gas}}$ is known. We derive $[\text{Si}/\text{H}]_{\text{dust}}$ either from $[\text{Si}/\text{H}]_{\text{ISM}} - [\text{Si}/\text{H}]_{\text{gas}}$ or from the Kramers-Kronig relation which relates the wavelength-integrated extinction to the total dust volume, where $[\text{Si}/\text{H}]_{\text{ISM}}$ is the interstellar silicon reference abundance and taken to be that of proto-Sun or B stars. We also derive $[\text{Si}/\text{H}]_{\text{dust}}$ from fitting the observed extinction curves with a mixture of amorphous silicates and graphitic grains. We find that in all three cases $[\text{Si}/\text{H}]_{\text{dust}}$ shows no correlation with the 2175 Å bump, while the carbon depletion $[\text{C}/\text{H}]_{\text{dust}}$ tends to correlate with the 2175 Å bump. This supports carbon grains instead of silicates as the possible carrier of the 2175 Å bump. We also find that neither $[\text{Si}/\text{H}]_{\text{dust}}$ nor $[\text{C}/\text{H}]_{\text{dust}}$ alone correlates with the far-UV extinction, suggesting that the far-UV extinction is a combined effect of small carbon grains and silicates.

Subject headings: dust, extinction — ISM: abundances — ISM: clouds

¹Department of Physics and Astronomy, University of Missouri, Columbia, MO 65211, USA; lia@missouri.edu

²Department of Science, Technology and Mathematics, Lincoln University, Jefferson City, MO 65101, USA; mishraa@lincolnu.edu

1. Introduction

Silicon, an abundant metal element in the Universe, is highly depleted from the gas phase in the diffuse interstellar medium (ISM; e.g., see Jenkins 1987, 2009) as revealed by the weak ultraviolet (UV) absorption lines of Si II, the dominant form of gas-phase silicon in the diffuse ISM (e.g., see van Steenberg & Shull 1988). The silicon atoms missing from the gas phase are thought to have been locked up in solid silicate dust grains (e.g., see Draine 1990). Silicate dust is ubiquitously seen in a wide variety of astrophysical environments through the absorption or emission spectral features arising from the Si–O and O–Si–O vibrational modes occurring respectively at 9.7 and 18 μm (see Henning 2010). In the diffuse ISM, these features are seen in absorption and their spectral profiles are smooth and lack fine structures, indicating a predominantly amorphous composition (Li & Draine 2001, Kemper et al. 2004, Li et al. 2007).

It has been well recognized that silicate grains are a major contributor to the interstellar extinction. Assuming all Si, Mg, and Fe elements of solar abundances (Asplund et al. 2009) are condensed in silicate dust with a stoichiometric composition of MgFeSiO_4 and a characteristic size of $a \approx 0.1 \mu\text{m}$, one can estimate the contribution of silicate dust to A_V , the extinction in the visual (V) band from

$$\begin{aligned} \left(\frac{A_V}{N_H} \right)_{\text{sil}} &\approx 1.086 \pi a^2 Q_{\text{ext}}(V) N_{\text{sil}} / N_H \\ &\approx \frac{1.086 \pi a^2 Q_{\text{ext}}(V) \left(\sum_{\text{X=Si,Mg,Fe}} [\text{X}/\text{H}]_{\odot} \mu_{\text{X}} + 4 [\text{Si}/\text{H}]_{\odot} \mu_{\text{O}} \right) m_{\text{H}}}{(4/3) \pi a^3 \rho_{\text{sil}}} \\ &\approx 3.25 \times 10^{-22} \text{ mag cm}^2, \end{aligned} \quad (1)$$

where N_H is the hydrogen column density, N_{sil} is the column density of silicate dust, $\rho_{\text{sil}} \approx 3.5 \text{ g cm}^{-3}$ is the mass density of silicate material, $Q_{\text{ext}}(V)$ is the visual extinction efficiency of submicron-sized silicate dust which is taken to be $Q_{\text{ext}}(V) \approx 1.5$ (see Li 2009), $[\text{X}/\text{H}]_{\odot}$ is the solar abundance (relative to H) of element X ($[\text{Si}/\text{H}]_{\odot} \approx 32.4 \pm 2.2 \text{ ppm}$, $[\text{Mg}/\text{H}]_{\odot} \approx 39.8 \pm 3.7 \text{ ppm}$, and $[\text{Fe}/\text{H}]_{\odot} \approx 31.6 \pm 2.9 \text{ ppm}$, Asplund et al. 2009), μ_{X} is the atomic weight of element X ($\mu_{\text{X}} \approx 16, 28, 24, 56$ for O, Si, Mg, and Fe, respectively), and $m_{\text{H}} \approx 1.66 \times 10^{-24} \text{ g}$ is the mass of a hydrogen atom. Eq. 1 estimates that silicate dust accounts for $\sim 60\%$ of the interstellar extinction for which $(A_V/N_H)_{\text{obs}} \approx 5.3 \times 10^{-22} \text{ mag cm}^2$ (Bohlin et al. 1978). Admittedly, this estimation is somewhat simplified since it is unlikely for interstellar silicate dust to have a single size of $a = 0.1 \mu\text{m}$. Being highly processed in the ISM by supernovae shocks through sputtering and shattering (Draine 2003), silicate dust is expected to have a range of sizes. Without knowing the silicate dust size distribution, Mishra & Li (2015) applied the Kramers-Kronig (KK) relation of Purcell (1969) to estimate that

silicate dust contributes to $\sim 48\%$ of the total wavelength-integrated interstellar extinction which is obtained by integrating the observed interstellar extinction over wavelength from the far-UV to the far infrared (IR). Indeed, all modern interstellar dust models assume amorphous silicate to be a major dust species (e.g., Mathis et al. 1977, Draine & Lee 1984, Duley et al. 1989, Désert et al. 1990, Siebenmorgen & Krügel 1992, Mathis 1996, Li & Greenberg 1997, Weingartner & Draine 2001, Li & Draine 2001a, Zubko et al. 2004, Jones et al. 2013, Wang et al. 2015).

In the Milky Way, the variation of the extinction A_λ with wavelength λ , known as the extinction curve or the extinction law, is characterized by a nearly linear increase with λ^{-1} in the near-IR, visible and near-UV, a broad absorption bump at about $\lambda^{-1} \approx 4.6 \mu\text{m}^{-1}$ ($\lambda \approx 2175 \text{ \AA}$), and a steep rise into the far-UV at $\lambda^{-1} \approx 10 \mu\text{m}^{-1}$, the shortest wavelength at which the dust extinction has been measured (see Li et al. 2015). Although a consensus has been achieved that silicate dust is a major contributor of the interstellar extinction, it is not exactly clear to what degree silicate dust is responsible for the UV and far-UV extinction.

Very recently, Haris et al. (2016) determined the gas-phase abundance of silicon ($[\text{Si}/\text{H}]_{\text{gas}}$) for 131 Galactic sightlines using archival data. Assuming the interstellar abundance of silicon to be solar (i.e., $[\text{Si}/\text{H}]_{\text{ISM}} = [\text{Si}/\text{H}]_{\odot}$), they derived the silicon depletion (i.e., $[\text{Si}/\text{H}]_{\text{dust}} = [\text{Si}/\text{H}]_{\text{ISM}} - [\text{Si}/\text{H}]_{\text{gas}}$) for each sightline. Haris et al. (2016) further examined the UV extinction curves of 16 sightlines (of these 131 sightlines) and explored the relation between the silicon depletion and the 2175 \AA extinction bump as well as the far-UV extinction rise. Although the derived Pearson correlation coefficients ($R \approx -0.42$ for the silicon depletion and the 2175 \AA bump, and $R \approx -0.32$ for the silicon depletion and the far-UV rise) are by no means substantial, they claimed that the silicon depletion positively “correlates” with the 2175 \AA bump and the far-UV extinction rise. They further argued that these “correlations” imply that silicon plays a significant role in both the 2175 \AA bump and the far-UV rise.

The 2175 \AA bump is the strongest spectroscopic extinction feature of the diffuse ISM (Draine 1989). Its carrier remains unidentified over half a century after its first detection (Stecher 1965). Although it is commonly attributed to small aromatic carbonaceous materials like nano-sized graphitic grains (e.g., see Stecher & Donn 1965, Draine & Malhotra 1993, Mathis 1994) or polycyclic aromatic hydrocarbon (PAH) molecules (Joblin et al. 1992, Li & Draine 2001a, Cecchi-Pestellini et al. 2008, Steglich et al. 2010, Mulas et al. 2013, Bekki et al. 2015), Duley (1985) and Steel & Duley (1987) ascribed the 2175 \AA bump to small silicates or (Mg, Si) oxides.

The 2175 \AA bump is an absorption feature with no scattered component, with the detection of scattering reported only in two reflection nebulae (Witt et al. 1986). While the strength and width of the 2175 \AA bump vary with environment, its peak wavelength is nearly

invariant (see Draine 1989). The nondetection of scattering and the stable peak wavelength imply that the carrier of the 2175 Å bump is sufficiently small (i.e., nano-sized) to be in the Rayleigh limit (Mathis 1994). If the 2175 Å bump is indeed related to silicate grains as suggested by Duley (1985), Steel & Duley (1987) and Haris et al. (2016), there would exist a population of nano-sized silicate grains in the diffuse ISM.

The far-UV extinction is also predominantly absorptive. General results concerning scattering by small particles indicate that the far-UV extinction arises from nano-sized grains (see Draine 1995), although the exact sizes of these grains can not be constrained by the far-UV extinction (see Wang et al. 2015). Therefore, the correlation between the silicon depletion and the far-UV extinction rise derived by Haris et al. (2016) also implies the existence of an appreciable number of nano silicate grains in the diffuse ISM.

Very recently, nano silicate grains are of renewed interest. Hoang et al. (2016) and Hensley & Draine (2017a) argued that the so-called “anomalous microwave emission” (AME), an important Galactic foreground of the cosmic microwave background radiation in the ~ 10 –100 GHz region, could arise from spinning nano-sized silicate grains. However, silicate nanoparticles will undergo single-photon heating in the ISM and emit at the 9.7 μm Si–O feature. The nondetection of the 9.7 μm emission feature in the diffuse ISM allows one to place an upper limit on the number of nano-sized interstellar silicate grains (see Li & Draine 2001b).

In light of these contradicting results or hypothesis (i.e., whether the 2175 Å extinction bump is due to small silicate grains or small carbonaceous grains, and whether nano-sized silicate grains are abundant in the diffuse ISM), we are motivated to explore the role of silicate grains in the interstellar UV extinction, with special attention paid to the 2175 Å extinction bump and the far-UV rise. To achieve this, we consider a larger sample of 46 sightlines for which both the UV extinction curves and the gas-phase $[\text{Si}/\text{H}]_{\text{gas}}$ abundances have been observationally determined (see §2). In contrast, Harris et al. (2016) only considered 16 sightlines. We first investigate the relation between the silicon depletion $[\text{Si}/\text{H}]_{\text{dust}}$ and the UV extinction by assuming an interstellar reference abundance¹ of $[\text{Si}/\text{H}]_{\text{ISM}}$ and deriving $[\text{Si}/\text{H}]_{\text{dust}}$ from subtracting from $[\text{Si}/\text{H}]_{\text{ISM}}$ off the gas-phase abundance $[\text{Si}/\text{H}]_{\text{gas}}$ (see §3). We then examine the relation between $[\text{Si}/\text{H}]_{\text{dust}}$ and the UV extinction by deriving $[\text{Si}/\text{H}]_{\text{dust}}$ from the KK relation of Purcell (1969) which relates the wavelength-integrated extinction to the total dust volume (see §4). Alternatively, we will also derive $[\text{Si}/\text{H}]_{\text{dust}}$ by modeling the observed extinction curve of each sightline in terms of the silicate-graphite model (see

¹The reference abundance (also known as “interstellar abundance”, or “cosmic abundance”) of an element is the total abundance of this element (both in gas and in dust).

§5) and then compare the derived $[\text{Si}/\text{H}]_{\text{dust}}$ with the observed UV extinction. Finally, the results are discussed in §6 and the major conclusions are summarized in §7.

2. The Sample

We compile from the literature all the Galactic sightlines for which both the UV extinction curves and the silicon gas-phase abundances $[\text{Si}/\text{H}]_{\text{gas}}$ have been observationally determined. Resultantly, we arrive at a sample of 46 sightlines (see Table 1) which is a subsample of the 131 sightlines of Haris et al. (2016). For each sightline, we take the $[\text{Si}/\text{H}]_{\text{gas}}$ abundance from Haris et al. (2016) and the extinction parameters c'_j ($j = 1, 2, 3, 4$), x_o and γ (see below) from Jenniskens & Greenberg (1993), Valencic et al. (2004), Lewis et al. (2005), and Gordon et al. (2009).

Following Valencic et al. (2004) and Gordon et al. (2009), we “construct” the UV extinction curve at $3.3 < \lambda^{-1} < 8.7 \mu\text{m}^{-1}$ of each sightline, as a function of $x \equiv 1/\lambda$ (in μm^{-1}), the inverse wavelength, from the following formula:

$$A_\lambda/A_V = c'_1 + c'_2 x + c'_3 D(x, \gamma, x_o) + c'_4 F(x) \quad . \quad (2)$$

This analytical formula consists of (i) a linear background term described by c'_1 and c'_2 , (ii) a Drude-profile term for the 2175 Å extinction bump (of peak x_o and FWHM γ) approximated as

$$D(x, \gamma, x_o) \equiv \frac{x^2}{(x^2 - x_o^2)^2 + x^2 \gamma^2} \quad , \quad (3)$$

and (iii) a far-UV nonlinear-rise term at $\lambda^{-1} > 5.9 \mu\text{m}^{-1}$ represented by

$$F(x) = \begin{cases} 0 , & x < 5.9 \mu\text{m}^{-1} \\ 0.5392 (x - 5.9)^2 + 0.05644 (x - 5.9)^3 , & x \geq 5.9 \mu\text{m}^{-1} \end{cases} \quad . \quad (4)$$

This parametrization, in which c'_3 and c'_4 respectively define the strength of the 2175 Å extinction bump and the strength of the nonlinear far-UV rise, was originally introduced by Fitzpatrick & Massa (1990; hereafter FM90) for the interstellar reddening

$$E(\lambda - V)/E(B - V) = R_V (A_\lambda/A_V - 1) = c_1 + c_2 x + c_3 D(x, \gamma, x_o) + c_4 F(x) \quad , \quad (5)$$

where $E(\lambda - V) \equiv A_\lambda - A_V$, $E(B - V) \equiv A_B - A_V$, A_B is the B -band extinction, and $R_V \equiv A_V/E(B - V)$ is the optical total-to-selective extinction ratio. The c_j parameters of FM90 are related to that of Valencic et al. (2004) and Gordon et al. (2009), c'_j , through

$$c'_j = \begin{cases} c_j/R_V + 1 , & j = 1 \\ c_j/R_V , & j = 2, 3, 4 \end{cases} \quad . \quad (6)$$

Finally, for each sightline we compute the optical/near-IR extinction at $0.3 < \lambda^{-1} < 3.3 \mu\text{m}^{-1}$ from the R_V -based CCM parametrization (see Cardelli et al. 1989). We then smoothly join the UV extinction at $\lambda^{-1} > 3.3 \mu\text{m}^{-1}$ to the optical/near-IR extinction at $\lambda^{-1} < 3.3 \mu\text{m}^{-1}$. In Figures 1–5 we show the UV/optical/near-IR extinction curves of 39 sightlines constructed as above. The extinction curves of the other seven sightlines have already been constructed and modeled previously (see Mishra & Li 2015).

3. Silicon Depletion Inferred from $[\text{Si}/\text{H}]_{\text{ISM}}$ and $[\text{Si}/\text{H}]_{\text{gas}}$

Elements in the ISM exist in the form of gas or dust. The interstellar gas-phase abundances of elements can be measured from their optical and UV spectroscopic absorption lines. The elements “missing” from the gas phase are bound up in dust grains, known as “interstellar depletion”. The dust-phase abundance of an element is derived by assuming a reference abundance and then from which subtracting off the gas-phase abundance.

Historically, the interstellar abundances of the dust-forming elements C, O, Mg, Si, Fe were commonly assumed to be solar. However, Lodders (2003) argued that the currently observed solar photospheric abundances (relative to H) must be lower than those of the proto-Sun because helium and other heavy elements may have settled toward the Sun’s interior since the time of its formation ~ 4.55 Gyr ago. Lodders (2003) further suggested that the protosolar abundances derived from the combined considerations of the present-day photospheric abundances and all the possible settling effects are more representative of the true interstellar abundances. On the other hand, it has also been argued that the interstellar abundances, because of their young ages, might be better represented by those of B stars and young F, G stars (e.g., see Snow & Witt 1995, 1996, Sofia & Meyer 2001). Therefore, in the following we will consider two sets of reference abundances for the dust-forming element: $[\text{X}/\text{H}]_{\text{ISM}} = [\text{X}/\text{H}]_{\odot}$ — the protosolar abundances of Lodders (2003), and $[\text{X}/\text{H}]_{\text{ISM}} = [\text{X}/\text{H}]_{\star}$ — the B-star abundances of Przybilla et al. (2008).

With $[\text{Si}/\text{H}]_{\text{ISM}} = [\text{Si}/\text{H}]_{\odot} \approx 40.7 \pm 1.9$ ppm of Lodders (2003) or $[\text{Si}/\text{H}]_{\text{ISM}} = [\text{Si}/\text{H}]_{\star} \approx 31.6 \pm 1.5$ ppm of Przybilla et al. (2008), we respectively derive the silicon depletion $[\text{Si}/\text{H}]_{\text{dust}} = [\text{Si}/\text{H}]_{\text{ISM}} - [\text{Si}/\text{H}]_{\text{gas}}$ for each sightline and then compare with the strength of the 2175 Å extinction bump (measured by c'_3) and the strength of the nonlinear far-UV rise (measured by c'_4). As shown in Figure 6, neither the 2175 Å bump nor the far-UV rise correlates with the silicon depletion.² This is true for both sets of reference-abundances: the exact value of

²Although somewhat arbitrary, we suggest that, for two variables to be considered to be (even weakly) correlated, the Pearson correlation coefficient (R) should at least exceed 0.5 (e.g., see

the interstellar silicon abundance is unimportant as long as we assume that it is the same for all directions. The correlation plots are identical for the two sets of reference-abundances except for a shift in ordinate.

4. Silicon Depletion Inferred from the Kramers-Kronig Relation

The approach discussed in §3 requires the knowledge of $[\text{Si}/\text{H}]_{\text{ISM}}$ and $[\text{Si}/\text{H}]_{\text{gas}}$. We note that $[\text{Si}/\text{H}]_{\text{gas}}$ is often difficult to measure since silicon is often highly depleted and the Si II absorption lines are rather weak. In this section we take an alternative, carbon-based approach which makes use of the KK relation of Purcell (1969) and does not require the knowledge of $[\text{Si}/\text{H}]_{\text{ISM}}$ and $[\text{Si}/\text{H}]_{\text{gas}}$.

Let $[\text{C}/\text{H}]_{\text{ISM}}$ be the total interstellar carbon abundance (relative to H), and $[\text{C}/\text{H}]_{\text{gas}}$ be the gas-phase carbon abundance of a given sightline. We derive the total volume (per H nucleon) of carbon dust for this sightline from

$$\frac{V_{\text{C}}}{\text{H}} = \left\{ [\text{C}/\text{H}]_{\text{ISM}} - [\text{C}/\text{H}]_{\text{gas}} \right\} \times 12 m_{\text{H}} / \rho_{\text{C}} \quad , \quad (7)$$

where ρ_{C} is the mass density of the carbon dust ($\rho_{\text{C}} \approx 2.24 \text{ g cm}^{-3}$ for graphite). We can apply the KK relation of Purcell (1969) to gain insight into the amount of extinction resulting from such an amount of carbon dust; particularly, the wavelength-integrated extinction is directly related to the dust volume through

$$\int_0^\infty \left(\frac{A_\lambda}{N_{\text{H}}} \right)_{\text{C}} d\lambda = 1.086 \times 3\pi^2 F_{\text{C}} \frac{V_{\text{C}}}{\text{H}} \quad , \quad (8)$$

where $(A_\lambda/N_{\text{H}})_{\text{C}}$ is the extinction (per H column) caused by carbon dust, and F_{C} is a dimensionless factor which depends only upon the grain shape and the static (zero-frequency) dielectric constant ε_0 of the grain material. For conducting, graphitic grains of moderately elongated shapes, Mishra & Li (2015) derived $F_{\text{C}} \approx 1.25$ (see their Figure 1).

Let $(A_\lambda/N_{\text{H}})_{\text{obs}}$ be the observed extinction (per H column) of a given sightline. If we assume that there are two major dust populations in the ISM — amorphous silicate and carbon dust, the extinction contributed by silicate dust, $(A_\lambda/N_{\text{H}})_{\text{sil}}$, can be obtained from

$$\int_0^\infty \left(\frac{A_\lambda}{N_{\text{H}}} \right)_{\text{sil}} d\lambda = \int_0^\infty \left(\frac{A_\lambda}{N_{\text{H}}} \right)_{\text{obs}} d\lambda - \int_0^\infty \left(\frac{A_\lambda}{N_{\text{H}}} \right)_{\text{C}} d\lambda \quad . \quad (9)$$

To account for such an amount of extinction, one requires a total silicate dust volume of

$$\frac{V_{\text{sil}}}{H} = \frac{\int_0^\infty (A_\lambda/N_{\text{H}})_{\text{sil}} d\lambda}{1.086 \times 3\pi^2 F_{\text{sil}}}, \quad (10)$$

where F_{sil} , like F_{C} , is a dimensionless factor. For moderately elongated silicate grains, $F_{\text{sil}} \approx 0.7$ (see Figure 1 in Mishra & Li 2015). We then derive the silicon depletion from the silicate dust volume

$$[\text{Si}/\text{H}]_{\text{dust}} = \frac{(V_{\text{sil}}/H) \rho_{\text{sil}}}{\mu_{\text{sil}} m_{\text{H}}}, \quad (11)$$

where $\mu_{\text{sil}} = 172$ is the molecular weight for MgFeSiO_4 . Therefore, we can infer $[\text{Si}/\text{H}]_{\text{dust}}$ from $[\text{C}/\text{H}]_{\text{ISM}}$, $[\text{C}/\text{H}]_{\text{gas}}$ and $(A_\lambda/N_{\text{H}})_{\text{obs}}$, without knowing $[\text{Si}/\text{H}]_{\text{ISM}}$ and $[\text{Si}/\text{H}]_{\text{gas}}$. Also, we do not need to know the exact dust properties (e.g., sizes, compositions) except for an assumed dust species we need to specify its mass density (ρ), molecular weight (μ) and whether the dust material is conducting (i.e., $\varepsilon_0 \rightarrow \infty$) or dielectric (i.e., ε_0 is finite).

Observationally, for many of our sightlines considered in this work the extinction per H nucleon is only known over a limited range of wavelengths (e.g., $0.3 < \lambda^{-1} < 8.7 \mu\text{m}^{-1}$). We approximate $\int_0^\infty (A_\lambda/N_{\text{H}})_{\text{obs}} d\lambda$ by $\int_{912\text{\AA}}^{1000\mu\text{m}} (A_\lambda/N_{\text{H}})_{\text{obs}} d\lambda$.³ We first use eq. 2 to extrapolate the UV extinction at $\lambda^{-1} < 8.7 \mu\text{m}^{-1}$ to $\lambda = 912\text{\AA}$.⁴ For $0.001 < \lambda^{-1} < 0.3 \mu\text{m}^{-1}$, we adopt the model A_λ/N_{H} values of Weingartner & Draine (2001; WD01) for the $R_V = 3.1$ diffuse ISM (see Figure 16 in Li & Draine 2001). This is justified since the near- and mid-IR extinction at $\lambda > 0.9 \mu\text{m}$ does not seem to vary much among different environments (see Wang et al. 2013, 2014). In Table 1 we tabulate the wavelength-integrated extinction for each sightline.

For the interstellar carbon reference abundance, similar to silicon in §3, we also consider two sets of reference abundances: $[\text{C}/\text{H}]_{\text{ISM}} = [\text{C}/\text{H}]_{\odot} \approx 288 \pm 27$ ppm — the protosolar abundance of Lodders (2003), and $[\text{C}/\text{H}]_{\text{ISM}} = [\text{C}/\text{H}]_{\star} \approx 214 \pm 20$ ppm — the B-star abundance of Przybilla et al. (2008). The gas-phase $[\text{C}/\text{H}]_{\text{gas}}$ abundance are not known for all sightlines. We estimate $[\text{C}/\text{H}]_{\text{gas}}$ from the hydrogen number density n_{H} , using the four-parameter Boltzmann function originally proposed by Jenkins et al. (1986) and subsequently modified

³The silicon depletion derived from $\int_{912\text{\AA}}^{1000\mu\text{m}} (A_\lambda/N_{\text{H}})_{\text{obs}} d\lambda$ is a lower limit since $\int_{912\text{\AA}}^{1000\mu\text{m}} (A_\lambda/N_{\text{H}})_{\text{obs}} d\lambda < \int_0^\infty (A_\lambda/N_{\text{H}})_{\text{obs}} d\lambda$.

⁴Gordon et al. (2009) studied the extinction curves of 75 Galactic sightlines obtained with the *Far Ultraviolet Spectroscopic Explorer* (FUSE) at $905 < \lambda < 1187\text{\AA}$ and the *International Ultraviolet Explorer* (IUE) at $1150 < \lambda < 3300\text{\AA}$. They found that the extrapolation of the UV extinction at $3.3 < \lambda^{-1} < 8.7 \mu\text{m}^{-1}$ obtained by IUE is generally consistent with the far-UV extinction at $8.4 < \lambda^{-1} < 11 \mu\text{m}^{-1}$ obtained by FUSE.

by Cartledge et al. (2004, 2006):

$$[\text{C}/\text{H}]_{\text{gas}} = [\text{C}/\text{H}]_{\text{cold}} + \frac{[\text{C}/\text{H}]_{\text{warm}} - [\text{C}/\text{H}]_{\text{cold}}}{1 + \exp \{ \log_{10} (n_{\text{H}}/n_0) / m \}} , \quad (12)$$

where $[\text{C}/\text{H}]_{\text{warm}}$ and $[\text{C}/\text{H}]_{\text{cold}}$ are respectively the carbon gas-phase abundance levels for low and high mean sightline densities, n_0 is a parameter with a dimension of hydrogen number density, and m is a dimensionless parameter.⁵ As shown in Figure 7, with $[\text{C}/\text{H}]_{\text{warm}} \approx 480 \pm 48$ ppm, $[\text{C}/\text{H}]_{\text{cold}} \approx 100.34 \pm 14.63$ ppm, $\log_{10} (n_0/\text{cm}^{-3}) \approx -0.919 \pm -0.103$, and $m \approx 0.33 \pm 0.12$, the Boltzmann-like function fits reasonably well the $n_{\text{H}}-[\text{C}/\text{H}]_{\text{gas}}$ relation for those sightlines of which both n_{H} and $[\text{C}/\text{H}]_{\text{gas}}$ are known. For those sightlines of which n_{H} (but not $[\text{C}/\text{H}]_{\text{gas}}$) has been observationally determined, we estimate the gas-phase $[\text{C}/\text{H}]_{\text{gas}}$ abundance from the hydrogen number density n_{H} and list in Table 2.

With $(A_{\lambda}/N_{\text{H}})_{\text{obs}}$ constructed as above and $[\text{C}/\text{H}]_{\text{gas}}$ estimated from n_{H} , we now use the KK relation of Purcell (1969) to derive the silicon depletions $[\text{Si}/\text{H}]_{\text{dust}}$ for all 46 sightlines and then compare $[\text{Si}/\text{H}]_{\text{dust}}$ with the UV extinction. As shown in Figure 8, $[\text{Si}/\text{H}]_{\text{dust}}$ does not correlate with c'_3 (i.e., the 2175 Å extinction bump), and nor does it correlate with c'_4 (i.e., the far-UV extinction rise). This is true no matter whichever is adopted as the interstellar reference abundance — the protosolar C/H abundance or the B-star C/H abundance. As already mentioned in §3, the exact value of the interstellar silicon abundance does not affect the correlation coefficient but causes a shift in ordinate.

So far, for the carbon dust species we are confined to graphite. However, this is actually unnecessary. After all, the KK approach does not really involve the optical properties and the size distribution of graphite. All we have used are the mass density of graphite ($\rho_{\text{gra}} \approx 2.24 \text{ g cm}^{-3}$) and the dimensionless factor F_{C} . If we consider amorphous carbon instead of graphite, the same conclusion will be drawn except the available carbon dust volume will be increased by a factor of $\rho_{\text{gra}}/\rho_{\text{ac}}$, where $\rho_{\text{ac}} \approx 1.8 \text{ g cm}^{-3}$ is the mass density of amorphous carbon. As illustrated in Figure 1 of Mishra & Li (2015), for moderately elongated grains, the dimensionless F_{C} factor of amorphous carbon ($F_{\text{C}} \approx 1.20$) differs only by $\sim 5\%$ from that of graphite ($F_{\text{C}} \approx 1.25$).

⁵We note that there was a typo in the expressions of Cartledge et al. (2004, 2006): the term $(n_{\text{H}} - n_0)$ in eq. 1 of Cartledge et al. (2004) and eq. 1 of Cartledge et al. (2006) should actually be $(\log_{10} n_{\text{H}} - \log_{10} n_0)$.

5. Silicon Depletion Inferred from Interstellar Extinction Modeling

The silicon depletion $[\text{Si}/\text{H}]_{\text{dust}}$ derived from the KK relation of Purcell (1969) in §4 is independent of any exact dust models except we just need to assume that the observed extinction is caused by silicate dust and carbon dust and specify the mass densities of the relevant dust materials and the static dielectric constant ε_0 which, together with the grain shape, determines the dimensionless factor F_C or F_{sil} .

We now derive the silicon depletion from fitting the observed extinction curve for each sightline. We consider the silicate-graphite interstellar grain model which consists of two separate dust components: amorphous silicate and graphite (Mathis et al. 1977, Draine & Lee 1984). We adopt an exponentially-cutoff power-law size distribution for both components: $dn_i/da = n_{\text{H}} B_i a^{-\alpha_i} \exp(-a/a_{c,i})$ for the size range of $50 \text{ \AA} < a < 2.5 \mu\text{m}$, where a is the spherical radius of the dust, dn_i is the number density of dust of type i with radii in the interval $[a, a + da]$, α_i and $a_{c,i}$ are respectively the power index and exponential cutoff size for dust of type i , and B_i is the constant related to the total amount of dust of type i . The total extinction per H column at wavelength λ is given by

$$A_{\lambda}/N_{\text{H}} = 1.086 \sum_i \int da \frac{1}{n_{\text{H}}} \frac{dn_i}{da} C_{\text{ext},i}(a, \lambda), \quad (13)$$

where the summation is over the two grain types (i.e., silicate and graphite), N_{H} is the hydrogen column density, and $C_{\text{ext},i}(a, \lambda)$ is the extinction cross section of grain type i of size a at wavelength λ which can be calculated from Mie theory (Bohren & Huffman 1983) using the dielectric functions of “astronomical” silicate and graphite of Draine & Lee (1984).

In fitting the extinction curve, for a given sightline, we have six parameters: the size distribution power indices α_{S} and α_{C} for silicate and graphite, respectively; the exponential cutoff sizes $a_{c,\text{S}}$ and $a_{c,\text{C}}$, respectively; and B_{S} and B_{C} . We derive the silicon and carbon depletions from

$$[\text{Si}/\text{H}]_{\text{dust}} = (n_{\text{H}} B_{\text{S}} / 172 m_{\text{H}}) \int da (4\pi/3) a^3 \rho_{\text{sil}} a^{-\alpha_{\text{S}}} \exp(-a/a_{c,\text{S}}) \quad , \quad (14)$$

$$[\text{C}/\text{H}]_{\text{dust}} = (n_{\text{H}} B_{\text{C}} / 12 m_{\text{H}}) \int da (4\pi/3) a^3 \rho_{\text{gra}} a^{-\alpha_{\text{C}}} \exp(-a/a_{c,\text{C}}) \quad , \quad (15)$$

where we assume a stoichiometric composition of MgFeSiO_4 for amorphous silicate.

For a given sightline, we seek the best fit to the extinction between $0.3 \mu\text{m}^{-1}$ and $8 \mu\text{m}^{-1}$ by varying the size distribution power indices α_{S} and α_{C} , and the upper cutoff size parameters $a_{c,\text{S}}$ and $a_{c,\text{C}}$. Following WD01, we evaluate the extinction at 100 wavelengths λ_i , equally

spaced in $\ln \lambda$. We use the Levenberg-Marquardt method (Press et al. 1992) to minimize χ^2 which gives the error in the extinction fit:

$$\chi^2 = \sum_i \frac{(\ln A_{\text{obs}} - \ln A_{\text{mod}})^2}{\sigma_i^2} \quad , \quad (16)$$

where $A_{\text{obs}}(\lambda_i)$ is the observed extinction at wavelength λ_i , $A_{\text{mod}}(\lambda_i)$ is the extinction computed for the model at wavelength λ_i (see eq. 13), and the σ_i are weights. Following WD01, we take the weights $\sigma_i^{-1} = 1$ for $1.1 < \lambda^{-1} < 8 \mu\text{m}^{-1}$ and $\sigma_i^{-1} = 1/3$ for $\lambda^{-1} < 1.1 \mu\text{m}^{-1}$.

In Figures 1–5 we show the model fits for 39 sightlines. The other seven sightlines have already been modeled in Mishra & Li (2015), in a similar manner. It can be seen from these figures that a simple mixture of silicate and graphite closely reproduces the observed UV/optical/near-IR extinction of all 46 sightlines. The model parameters are tabulated in Table 2. In Figure 9 we explore the interrelations among the dust model parameters $a_{c,C}$, α_C , $a_{c,S}$ and α_S . No correlations are found, implying that they are independent. The other two parameters B_S and B_C respectively measure the amounts of silicate dust and graphite dust (see eqs. 14, 15) required to account for the observed extinction. They are not correlated with each other or with $a_{c,C}$, α_C , $a_{c,S}$ and α_S .

In Figure 10a we examine the correlation between the strength of the 2175 Å extinction bump (c'_3) with the silicon depletion ($[\text{Si}/\text{H}]_{\text{dust}}$) derived from fitting the observed extinction (see eq. 14). With a Pearson correlation coefficient of $R \approx -0.03$ and a Kendall $\tau \approx -0.05$ and $p \approx 0.61$, it is clear that the silicon depletion does not correlate with the 2175 Å bump. In contrast, the carbon depletion ($[\text{C}/\text{H}]_{\text{dust}}$) derived from fitting the observed extinction (see eq. 15) exhibits a positive correlation of $R \approx 0.77$, $\tau \approx 0.57$ and $p \approx 2.84 \times 10^{-8}$ with the 2175 Å bump (see Figure 10b). This is not unexpected since the silicate-graphite model assigns the 2175 Å bump to graphite. As illustrated in Figures 1–5, the 2175 Å bump arises exclusively from graphite.

We have also explored the relation between $[\text{Si}/\text{H}]_{\text{dust}}$ and the strength of the nonlinear far-UV extinction rise (c'_4). As shown in Figure 10c, no correlation is found. Similarly, Figure 10d compares $[\text{C}/\text{H}]_{\text{dust}}$ with c'_4 and also reveals no strong correlation. However, the correlation coefficient for $[\text{C}/\text{H}]_{\text{dust}}$ and c'_4 ($R \approx 0.44$) is appreciably higher than that for $[\text{Si}/\text{H}]_{\text{dust}}$ and c'_4 ($R \approx 0.10$). At a first glance, this is somewhat surprising since a visual inspection of Figures 1–5 indicates that silicates appear to be a more important contributor to the far-UV extinction than graphite. We believe that this is related to the nature of c'_4 : it arises from the FM mathematical separation of the UV extinction into a linear “background” at $\lambda^{-1} > 3.3 \mu\text{m}^{-1}$ and a nonlinear far-UV rise at $\lambda^{-1} > 5.9 \mu\text{m}^{-1}$. By design, c'_4 only measures the far-UV nonlinear rise, not the whole UV extinction. As illustrated in Figures 1–5, for many sightlines the extinction calculated from silicate grains

somewhat resembles a linear “background”. This explains why $[\text{Si}/\text{H}]_{\text{dust}}$ does not correlate with c'_4 . On the other hand, although $[\text{C}/\text{H}]_{\text{dust}}$ seems to show a somewhat better correlation with c'_4 , the correlation is still very weak or at most marginal. This suggests that the far-UV extinction is more likely a combined effect of small silicates and small graphitic grains.

Finally, we examine how $[\text{Si}/\text{H}]_{\text{dust}}$ and $[\text{C}/\text{H}]_{\text{dust}}$ vary with R_V^{-1} . As shown in Figures 10e,f, while $[\text{Si}/\text{H}]_{\text{dust}}$ exhibits no correlation with R_V^{-1} , with a Pearson correlation coefficient of $R \approx 0.54$, $[\text{C}/\text{H}]_{\text{dust}}$ appears to moderately correlate with R_V^{-1} . This may merely reflect the fact that the 2175 Å bump tends to correlate with R_V^{-1} (see Figure 7 of Cardelli et al. 1989) while the 2175 Å bump also correlates with $[\text{C}/\text{H}]_{\text{dust}}$ (see Figure 10b). Cardelli et al. (1989) demonstrated that not only the 2175 Å bump correlates with R_V^{-1} , but also the extinction at *any* other wavelengths within the near-IR to the far-UV correlates equally well with R_V^{-1} (see their Figures 1, 2). This implies that $[\text{C}/\text{H}]_{\text{dust}}$ must correlate not only with the 2175 Å bump, but also and equally well with the extinction at other wavelengths. We stress that this is not necessarily inconsistent with the lack of correlation between $[\text{C}/\text{H}]_{\text{dust}}$ and c'_4 (see Figure 10d) since, as discussed above, c'_4 is not an accurate measure of the whole UV extinction but the far-UV nonlinear rise.

6. Discussion

In previous sections we have demonstrated that, using both dust model-independent and model-dependent approaches, the UV extinction (including the 2175 Å bump and the far-UV nonlinear rise) of 46 sightlines of which R_V ranges from ~ 2.4 to ~ 5.8 does not correlate with the silicon depletion. This is in stark contrast to Haris et al. (2016) who reported a positive correlation between the silicon depletion and the 2175 Å bump and the far-UV rise. Haris et al. (2016) derived such a correlation from a smaller sample of 16 sightlines. They adopted an interstellar reference abundance of $[\text{Si}/\text{H}]_{\text{ISM}} \approx 33.9$ ppm of Lodders et al. (2009) and derived $[\text{Si}/\text{H}]_{\text{dust}}$ by subtracting off the gas-phase abundance ($[\text{Si}/\text{H}]_{\text{gas}}$) from $[\text{Si}/\text{H}]_{\text{ISM}}$. Our approach described in §3 is similar to Haris et al. (2016) but for a larger sample of 46 sightlines. Also, we should note that the correlations derived by Haris et al. (2016), with $R \approx -0.42$ and $p < 0.10$ for the $[\text{Si}/\text{H}]_{\text{dust}}-c'_3$ relation and $R \approx -0.32$ and $p < 0.23$ for the $[\text{Si}/\text{H}]_{\text{dust}}-c'_4$ relation, were rather marginal.

In §5 we have shown that, based on the silicate-graphite model, the carbon depletion is correlated with the 2175 Å extinction bump, supporting the hypothesis of PAHs and/or small graphitic grains as the carrier of the 2175 Å bump (e.g., see Stecher & Donn 1965, Draine & Malhotra 1993, Mathis 1994, Joblin et al. 1992, Li & Draine 2001a, Cecchi-Pestellini et al. 2008, Steglich et al. 2010, Mulas et al. 2013, Bekki et al. 2015). This is not surprising

since this model-dependent approach, *a priori*, attributes the 2175 Å bump to graphite.⁶ To overcome this shortcoming, we could derive $[C/H]_{\text{dust}}$ by subtracting $[C/H]_{\text{gas}}$ (see §4 and eq. 12) from $[C/H]_{\text{ISM}}$, with the interstellar reference abundance of carbon taken to be either protosolar (Lodders 2003) or that of B stars (Przybilla et al. 2008). This approach does not need a prior assignment of the 2175 Å bump carrier. As illustrated in Figures 11a, with a Pearson correlation coefficient of $R \approx 0.51$, $[C/H]_{\text{dust}}$ shows a weak tendency of correlating with c'_3 . This is true either the protosolar C/H abundance or the C/H abundance of B stars is adopted as the interstellar reference abundance. We note that in our previous work for a sample of 16 sightlines (see Mishra & Li 2015), a better correlation was derived for $[C/H]_{\text{dust}}$ and c'_3 . We speculate that the correlation derived here is complicated by the fact that the gas-phase $[C/H]_{\text{gas}}$ abundance is not known for all the 46 sightlines considered here; instead, eq. 12 is used to estimate $[C/H]_{\text{gas}}$ for those sightlines for which $[C/H]_{\text{gas}}$ is not observationally determined. In contrast, for the 16 lines of sight considered in Mishra & Li (2015), the gas-phase $[C/H]_{\text{gas}}$ abundance is known for every line of sight.

Alternatively, we can also derive the carbon depletion $[C/H]_{\text{dust}}$ required to account for the observed extinction from the KK relation of Purcell (1969). Similar to the approach described in §4, by assuming an interstellar silicon reference abundance of $[Si/H]_{\text{ISM}}$, for a given sightline of known $[Si/H]_{\text{gas}}$ we first derive the total volume (per H nucleon) of silicate dust from

$$\frac{V_{\text{sil}}}{H} = \left\{ [Si/H]_{\text{ISM}} - [Si/H]_{\text{gas}} \right\} \times \mu_{\text{sil}} m_H / \rho_{\text{sil}} \quad , \quad (17)$$

where $\mu_{\text{sil}} = 172$ if we assume a stoichiometric composition of MgFeSiO_4 . By applying the KK relation of Purcell (1969), we obtain the wavelength-integrated extinction of silicate origin from the silicate dust volume through

$$\int_0^\infty \left(\frac{A_\lambda}{N_H} \right)_{\text{sil}} d\lambda = 1.086 \times 3\pi^2 F_{\text{sil}} \frac{V_{\text{sil}}}{H} \quad . \quad (18)$$

Again, if we assume amorphous silicate and carbon dust as two major dust populations in the ISM, we derive the extinction contributed by carbon dust from

$$\int_0^\infty \left(\frac{A_\lambda}{N_H} \right)_C d\lambda = \int_0^\infty \left(\frac{A_\lambda}{N_H} \right)_{\text{obs}} d\lambda - \int_0^\infty \left(\frac{A_\lambda}{N_H} \right)_{\text{sil}} d\lambda \quad . \quad (19)$$

We then apply the KK relation again to deduce the total volume of carbon dust required to account for the carbon-originated extinction $\int_0^\infty (A_\lambda/N_H)_C d\lambda$:

$$\frac{V_C}{H} = \frac{\int_0^\infty (A_\lambda/N_H)_C d\lambda}{1.086 \times 3\pi^2 F_C} \quad . \quad (20)$$

⁶The dielectric functions of “astronomical” silicate and graphite of Draine & Lee (1984) adopted in §5 were designed in such a way that graphite causes the 2175 Å extinction bump.

Finally, from the carbon dust volume we derive the carbon depletion to be

$$[\text{C}/\text{H}]_{\text{dust}} = \frac{(V_{\text{C}}/\text{H}) \rho_{\text{C}}}{12m_{\text{H}}} . \quad (21)$$

This approach does not require the knowledge of the unknown interstellar carbon reference abundance $[\text{C}/\text{H}]_{\text{ISM}}$ and the gas-phase carbon abundance $[\text{C}/\text{H}]_{\text{gas}}$. The latter is also unknown for some sightlines and in previous sections, it was estimated from n_{H} through eq. 12.

For each sightline, assuming the interstellar silicon reference abundance to be either protosolar ($[\text{Si}/\text{H}]_{\text{ISM}} = [\text{Si}/\text{H}]_{\odot} \approx 40.7 \pm 1.9$ ppm; Lodders 2003) or like B stars ($[\text{Si}/\text{H}]_{\text{ISM}} = [\text{Si}/\text{H}]_{\star} \approx 31.6 \pm 1.5$ ppm; Przybilla et al. 2008) and taking the observed extinction $(A_{\lambda}/N_{\text{H}})_{\text{obs}}$ constructed in §5 and the observationally determined gas-phase silicon abundance $[\text{Si}/\text{H}]_{\text{gas}}$, we derive the carbon depletion $[\text{C}/\text{H}]_{\text{dust}}$ from eqs. 17–21 and then compare with the 2175 Å extinction bump (measured by c'_3). As shown in Figures 12a, with a Pearson correlation coefficient of $R \approx 0.53$, $[\text{C}/\text{H}]_{\text{dust}}$ tends to weakly correlate with c'_3 . Again, this is true either the protosolar Si/H abundance or the Si/H abundance of B stars is adopted as the interstellar reference abundance. This supports the hypothesis of some sorts of carbonaceous grains (e.g., graphite or PAHs) as the possible carriers of the 2175 Å bump, while the lack of correlation between the silicon depletion and the 2175 Å bump (see §3, §4, and §5) argues against small silicates or (Mg, Si) oxides as its carrier (Duley 1985, Steel & Duley 1987, Parvathi et al. 2012, Haris et al. 2016).

We also show in Figure 11b and Figure 12b that $[\text{C}/\text{H}]_{\text{dust}}$ does not correlate with the far-UV extinction rise as measured by c'_4 . This, together with the lack of correlation of $[\text{Si}/\text{H}]_{\text{dust}}$ with c'_4 (see §3, §4, and §5), suggests that neither small silicate grains nor small carbon grains alone account for the far-UV extinction rise, instead, it must be their combined effects. Indeed, as illustrated in Figure 3 of Xiang et al. (2017), the silicate-graphite-PAH model of WD01 requires both silicate grains of sizes $a \lesssim 250$ Å and graphitics grains or PAHs of $a \lesssim 250$ Å to appreciably contribute to the far-UV extinction. Moreover, the nondetection of correlation between the 2175 Å bump and the far-UV rise (see Greenberg & Chlewicki 1983, Rouleau et al. 1997, Xiang et al. 2017) also implies that the bump carriers are not a dominant contributor of the far-UV extinction. Finally, we note that, while the FM parametrization provides an excellent mathematical description of the UV extinction at $\lambda^{-1} > 3.3 \mu\text{m}^{-1}$, the distinction between the linear rise (measured by c'_1 and c'_2) and the nonlinear far-UV rise (measured by c'_4) probably has little physical significance since there is no substance known that shows the corresponding extinction of any of them. We suggest that the decomposition scheme originally proposed by Greenberg (1973) and very recently revisited by Xiang et al. (2017) may be a better characterization of the far-UV extinction. According to this decomposition scheme, any observed interstellar extinction curve can be decomposed into three parts: (i) a near-IR/visible component which flattens off in the UV

and far-UV, (ii) a bump at 2175 Å, and (iii) a far-UV component. It would be interesting to explore the relations of the carbon and silicon depletions with these decomposed extinction components.

To summarize, we have demonstrated the refutation of Haris et al. (2016) by expanding our earlier study (Mishra & Li 2015) to provide a better understanding of the extinction curve and show that the 2175 Å extinction does not correlate with the silicon depletion. We should stress that, although this study supports the hypothesis of graphite or PAHs as the possible carriers of the 2175 Å bump, it has not yet necessarily approved this hypothesis. Neither the carrier of the bump nor those of the far-UV rise are yet assigned. The attribution of the far-UV extinction to a mixture of small carbon grains and small silicates also remains hypothetical. The 2175 Å bump could well be caused by a separate population of grains other than graphite or PAHs, e.g., carbon buckyonions (Chhowalla et al. 2003, Iglesias-Groth et al. 2003, Ruiz et al. 2005, Li et al. 2008). The far-UV extinction could also be partly contributed by iron nanoparticles (e.g., see Hensley & Draine 2017b). Also, the division of the UV extinction curve into a three-component scheme is by no means physical.

Finally, we show in Figure 13 the variations of A_λ/A_V with R_V^{-1} for $\lambda = 0.12 \mu\text{m}$, $0.15 \mu\text{m}$, $0.22 \mu\text{m}$, $0.28 \mu\text{m}$, $0.33 \mu\text{m}$, and $0.70 \mu\text{m}$. One can see that at $\lambda = 0.12 \mu\text{m}$, $0.15 \mu\text{m}$, $0.22 \mu\text{m}$, and $0.28 \mu\text{m}$, there is a good linear relationship between A_λ/A_V and R_V^{-1} , confirming the earlier findings of Cardelli et al. (1989). At $\lambda = 0.33 \mu\text{m}$ and $0.70 \mu\text{m}$, A_λ/A_V appears to correlate with R_V^{-1} much more weakly (if at all). This could be related to the use of A_V for normalizing the extinction. As illustrated in Figure 2 of Cardelli et al. (1989), if normalized to the *I*-band extinction at $\lambda \approx 0.90 \mu\text{m}$, the extinction, expressed as A_λ/A_I , shows a clear relation with R_V^{-1} for all wavelengths at $\lambda < 0.90 \mu\text{m}$.⁷

The correlation between R_V^{-1} and the extinction at *any* wavelength from the optical to the far-UV suggests the existence of a common process that simultaneously modifies all parts of the extinction curve (see §4 in Cardelli et al. 1989). As the extinction at a particular wavelength λ is dominated by grains of a particular size $a \sim \lambda/2\pi$ (see Li 2009), the fact that A_λ/A_V correlates with R_V^{-1} at all wavelengths implies that the process which produces changes in extinction must operate effectively and rather continuously over most of the range of grain sizes (except the largest sizes since the near- and mid-IR extinction seems to show little dependence with environments; see Wang et al. 2014, Xue et al. 2016). To examine this, we explore how the mean grain sizes derived in §5 from fitting the observed extinction curves vary with R_V^{-1} .

⁷The extinction law at $\lambda \gtrsim 0.90 \mu\text{m}$ appears to vary very little with environments (e.g., see Martin & Whittet 1990, Wang & Jiang 2014, Wang et al. 2013).

Let $\langle a \rangle_{\text{sil}}$ and $\langle a \rangle_{\text{gra}}$ respectively be the mean sizes of the silicate and graphite grains. For a given weighting factor $\omega(a)$, we derive $\langle a \rangle_{\text{sil}}$ and $\langle a \rangle_{\text{gra}}$ from the size distribution parameters determined in §5 as follows:

$$\langle a \rangle_{\text{sil}} = \frac{\int da \omega(a) a^{1-\alpha_s} \exp(-a/a_{c,s})}{\int da \omega(a) a^{-\alpha_s} \exp(-a/a_{c,s})}, \quad \langle a \rangle_{\text{gra}} = \frac{\int da \omega(a) a^{1-\alpha_C} \exp(-a/a_{c,C})}{\int da \omega(a) a^{-\alpha_C} \exp(-a/a_{c,C})}. \quad (22)$$

We shall consider three kinds of weighting factors: $\omega(a) = a^2$ (i.e., weighted by grain surface area), $\omega(a) = a^3$ (i.e., weighted by grain mass or volume), and $\omega(a) = C_{\text{ext}}(a, \lambda)$ (i.e., weighted by extinction cross section at wavelength λ). We define the overall mean grain size as the average of $\langle a \rangle_{\text{sil}}$ and $\langle a \rangle_{\text{gra}}$, weighted by the mass fraction of each dust component:

$$\langle a \rangle = \langle a \rangle_{\text{sil}} \frac{\mu_{\text{sil}} [\text{Si}/\text{H}]_{\text{dust}}}{\mu_{\text{C}} [\text{C}/\text{H}]_{\text{dust}} + \mu_{\text{sil}} [\text{Si}/\text{H}]_{\text{dust}}} + \langle a \rangle_{\text{gra}} \frac{\mu_{\text{C}} [\text{C}/\text{H}]_{\text{dust}}}{\mu_{\text{C}} [\text{C}/\text{H}]_{\text{dust}} + \mu_{\text{sil}} [\text{Si}/\text{H}]_{\text{dust}}}, \quad (23)$$

where the silicon ($[\text{Si}/\text{H}]_{\text{dust}}$) and carbon depletions ($[\text{C}/\text{H}]_{\text{dust}}$) are determined in §5 from modeling the observed extinction curves (see eqs. 14, 15 and Table 2).

In Figure 14 we show the area- and mass-weighted mean grain sizes ($\langle a \rangle$) as a function of R_V^{-1} . One can see that the mean sizes clearly anti-correlate with R_V^{-1} (i.e., in denser regions of larger R_V values, on an average, the grains are larger). As illustrated in Figure 15, the anti-correlation between $\langle a \rangle$ and R_V^{-1} is also seen for the $C_{\text{ext}}(a, \lambda)$ -weighted mean grain sizes, with $C_{\text{ext}}(a, \lambda)$ calculated at various wavelengths from the optical to the far-UV. This demonstrates that whatever processes modify the dust size distribution in one regime and the extinction at one wavelength must act in a rather systematic fashion over the entire size distribution and the extinction over the entire wavelength range from the optical to the far-UV. However, it is not clear what processes play a dominant role in regulating the extinction curve and the dust sizes (see Cardelli et al. 1989).

7. Conclusion

We have studied the extinction and dust depletion in 46 Galactic sightlines of which R_V ranges from ~ 2.4 to ~ 5.8 in order to probe the role of silicon in the UV extinction, particularly the 2175 Å extinction bump. These sightlines, with their UV/optical/near-IR extinction, gas-phase silicon abundances, and hydrogen column densities observationally determined, allow us to quantitatively explore the relations between the silicon depletion and the UV extinction. Our principal results are as follows:

1. By deriving the silicon depletion $[\text{Si}/\text{H}]_{\text{dust}}$ from subtracting the observed gas-phase silicon abundance $[\text{Si}/\text{H}]_{\text{gas}}$ from the assumed interstellar silicon reference abundance

$[\text{Si}/\text{H}]_{\text{ISM}}$, we find that $[\text{Si}/\text{H}]_{\text{dust}}$ is not correlated either with the 2175 Å extinction bump or with the far-UV extinction rise. This approach is independent of any dust models.

2. By deriving $[\text{Si}/\text{H}]_{\text{dust}}$ from the Kramers-Kronig relation which relates the wavelength-integrated extinction to the total dust volume, we also find no correlation between $[\text{Si}/\text{H}]_{\text{dust}}$ and the 2175 Å bump or the far-UV extinction rise. This approach is also model independent in the sense that it does not require the knowledge of the exact optical properties, composition and size distribution of the dust.
3. We have also derived $[\text{Si}/\text{H}]_{\text{dust}}$ as well as the carbon depletion $[\text{C}/\text{H}]_{\text{dust}}$ from fitting the observed UV/optical/near-IR extinction with a mixture of silicate dust and carbon dust. While no correlation is found between $[\text{Si}/\text{H}]_{\text{dust}}$ and the 2175 Å bump or between $[\text{Si}/\text{H}]_{\text{dust}}$ and the far-UV rise, $[\text{C}/\text{H}]_{\text{dust}}$ does show a positive correlation with the 2175 Å bump.
4. We have also derived $[\text{C}/\text{H}]_{\text{dust}}$ either from subtracting the gas-phase abundance $[\text{C}/\text{H}]_{\text{gas}}$ from the assumed interstellar reference abundance $[\text{C}/\text{H}]_{\text{ISM}}$ or from the Kramers-Kronig relation. In both cases we find that $[\text{C}/\text{H}]_{\text{dust}}$ tends to correlate with the 2175 Å bump (but not with the far-UV rise).
5. We conclude that some sorts of carbonaceous grains (e.g., graphite or PAHs) are the most plausible carrier of the 2175 Å bump, and silicates or (Mg, Si) oxides are unlikely responsible for the bump. Neither small silicate grains nor small carbon grains alone account for the the far-UV extinction rise, instead, it must be their combined effects.
6. We have shown that the extinction at *any* wavelength from the optical to the far-UV correlates with R_V^{-1} , consistent with the earlier findings of Cardelli et al. (1989). We have also found that the area-, mass-, or extinction-weighted mean grain size averaged over silicate dust and graphite dust anti-correlates with R_V^{-1} . This demonstrates that in the ISM the processes which modify the extinction at one wavelength and the grain size in one regime must also modify the extinction over the entire wavelength range and the grain size over the entire size range, although the exact processes remain unknown.

We thank B.T. Draine, B.W. Jiang, H. Kimura, A.N. Witt, G. Zhao and the anonymous referee for helpful discussions and comments. We are supported in part by NSF AST-1109039, NNX13AE63G, and NSFC 11173019, 11273022 and the University of Missouri Research Board.

REFERENCES

- Asplund, M., Grevesse, N., Sauval, A. J., & Scott, P. 2009, *ARA&A*, 47, 481
- Bekki, K., Hirashita, H., & Tsujimoto, T. 2015, *ApJ*, 810, 39
- Bohren, C. F., & Huffman, D. R. 1983, *Absorption and Scattering of Light by Small Particles* (New York: Wiley)
- Bohlin, R. C., Savage, B. D., & Drake, J. F. 1978, *ApJ*, 224, 132
- Cardelli, J. A., Clayton, G. C., & Mathis, J. S. 1989, *ApJ*, 345, 245 (CCM)
- Cartledge, S. I. B., Lauroesch, J. T., Meyer, D. M., & Sofia, U. J. 2004, *ApJ*, 613, 1037
- Cartledge, S. I. B., Lauroesch, J. T., Meyer, D. M., & Sofia, U. J. 2006, *ApJ*, 641, 327
- Cecchi-Pestellini, C., Mallocci, G., Mulas, G., Joblin, C., & Williams, D. A. 2008, *A&A*, 486, L25
- Chhowalla, M., Wang, H., Sano, N., Teo, K. B., Lee, S. B., & Amaratunga, G. A. 2003, *Phys. Rev. Lett.*, 90, 155504
- Désert, F.-X., Boulanger, F., & Puget, J. L. 1990, *A&A*, 237, 215
- Draine, B. T. 1989, in *IAU Symp. 135, Interstellar Dust*, ed. L. J. Allamandola & A. G. G. M. Tielens (Dordrecht: Kluwer), 313
- Draine, B. T. 1990, in *ASP Conf. Ser. 12, The Evolution of the Interstellar Medium*, ed. L. Blitz (San Francisco, CA: ASP), 193
- Draine, B. T. 1995, in *ASP Conf. Ser. 80, The Physics of the Interstellar Medium and Intergalactic Medium*, ed. A. Ferrara, C. F. McKee, C. Heiles, & P. R. Shapiro (San Francisco, CA: ASP), 133
- Draine, B.T. 2003, in *The Cold Universe, Saas-Fee Advanced Course Vol. 32*, ed. D. Pfenniger (Berlin: Springer-Verlag), 213
- Draine, B. T., & Lee, H. M. 1984, *ApJ*, 258, 89
- Draine, B. T., & Malhotra, S. 1993, *ApJ*, 414, 632
- Duley, W. W. 1985, *Ap&SS*, 112, 321
- Duley, W. W., Jones, A. P., & Williams, D. A. 1989, *MNRAS*, 236, 709

- Fitzpatrick, E. L., & Massa, D. 1990, *ApJS*, 72, 163
- Furton, D. G., Laiho, J. W., & Witt, A. N. 1999, *ApJ*, 526, 752
- Gnacinski, P., & Sikorski, J. 1999, *Acta Astron.*, 49, 577
- Gordon, K. D., Cartledge, S., & Clayton, G. C. 2009, *ApJ*, 705, 1320
- Greenberg, J.M. 1973, in *Molecules in the Galactic Environment*, ed. M. Gordon & L. Snyder (New York: Wiley), 93
- Greenberg, J. M., & Chlewicki, G. 1983, *ApJ*, 272, 563
- Gudennavar, S. B., Bubbly, S. G., Preethi, K., & Jayant, M. 2012, *ApJS*, 199, 8
- Haris, U., Parvathi, V. S., Gudennavar, S. B., et al. 2016, *AJ*, 151, 143
- Henning, Th. 2010, *ARA&A*, 48, 21
- Hensley, B. S., & Draine, B. T. 2017a, *ApJ*, 836, 179
- Hensley, B. S., & Draine, B. T. 2017b, *ApJ*, 836, 134
- Hoang, T., Vinh, N.-A., & Quynh Lan, N. 2016, *ApJ*, 824, 18
- Iglesias-Groth, S., Ruiz, A., Bretón, J., & Gomez Llorente, J. M. 2003, *J. Chem. Phys.*, 118, 7103
- Jenniskens, P., & Greenberg, J. M. 1993, *A&A*, 274, 439
- Jenkins, E. B. 1987, in *Interstellar Processes*, ed. D. J. Hollenbach & H. A. Thronson, Jr. (Dordrecht: Reidel), 533
- Jenkins, E.B. 2009, *ApJ*, 700, 1299
- Jenkins, E. B., Savage, B. D., & Spitzer, L. 1986, *ApJ*, 301, 355
- Joblin, C., Léger, A., & Martin, P. 1992, *ApJ*, 393, L79
- Jones, A. P., Fanciullo, L., Köhler, M., et al. 2013, *A&A*, 558, AA62
- Kemper, F., Vriend, W. J., & Tielens, A. G. G. M. 2004, *ApJ*, 609, 826
- Lewis, N. K., Cook, T. A., & Chakrabarti, S. 2005, *ApJ*, 619, 357

- Li, A. 2009, in *Small Bodies in Planetary Sciences*, ed. I. Mann, A. Nakamura, & T. Mukai (Berlin: Springer), 167
- Li, A., & Draine, B. T. 2001a, *ApJL*, 550, L213
- Li, A., & Draine, B. T. 2001b, *ApJ*, 554, 778
- Li, A., & Greenberg, J. M. 1997, *A&A*, 323, 566
- Li, A., Wang, S., Gao, J., & Jiang, B. W. 2015, in *Lessons from the Local Group – A Conference in Honour of David Block and Bruce Elmegreen*, eds. Freeman, K.C., Elmegreen, B.G., Block, D.L. & Woolway, M. (Springer: New York), 85 (arXiv: 1507.06604)
- Li, M. P., Zhao, G., & Li, A. 2007, *MNRAS*, 382, L26
- Lodders, K. 2003, *ApJ*, 591, 1220
- Lodders, K., Palme, H., & Gail, H.-P. 2009, *Landolt-Börnstein, New Series, Astronomy and Astrophysics* (Berlin: Springer), 4, 44 (arXiv:0901.1149)
- Martin, P. G., & Whittet, D. C. B. 1990, *ApJ*, 357, 113
- Mathis, J.S. 1994, *ApJ*, 422, 176
- Mathis, J.S. 1996, *ApJ*, 472, 643
- Mathis, J.S., Rumpl, W., & Nordsieck, K.H. 1977, *ApJ*, 217, 425
- Mishra, A., & Li, A., 2015, *ApJ*, 809, 120
- Mulas, G., Zonca, A., Casu, S., & Cecchi-Pestellini, C. 2013, *ApJS*, 207, 7
- Parvathi, V. S., Sofia, U.J., Murthy, J., & Babu. B. R. S. 2012, *ApJ*, 760, 36
- Press, W. H., Teukolsky, S. A., Vetterling, W. T., & Flannery, B. P. 1992, *Numerical Recipes in FORTRAN: The Art of Scientific Computing* (2nd ed.; Cambridge: Cambridge Univ. Press)
- Przybilla, N., Nieva, M. F., & Butler, K. 2008, *ApJ*, 688, L103
- Purcell, E. M. 1969, *ApJ*, 158, 433
- Rachford, B. L., Snow, T. P., Destree, J. D., et al. 2009, *ApJS*, 180, 125

- Rouleau, F., Henning, Th., & Stognienko, R. 1997, *A&A*, 322, 633
- Ruiz, A., Bretón, J., & Gomez Llorente, J. M. 2005, *Phys. Rev. Lett.*, 94, 105501
- Siebenmorgen, R., & Krügel, E. 1992, *A&A*, 259, 614
- van Steenberg, M. E., & Shull, J. M. 1988, *ApJ*, 330, 942
- Snow, T. P., & Witt, A. N. 1995, *Science*, 270, 1455
- Snow, T. P., & Witt, A. N. 1996, *ApJ*, 468, L65
- Sofia, U. J., & Meyer, D. M. 2001, *ApJ*, 558, L147
- Sofia, U. J., Lauroesch, J. T., Meyer, D. M., & Cartledge, S. I. B. 2004, *ApJ*, 605, 272
- Stecher, T. P. 1965, *ApJ*, 142, 1683
- Stecher, T. P., & Donn, B. 1965, *ApJ*, 142, 1681
- Steel, T. M., & Duley, W. W. 1987, *ApJ*, 315, 337
- Steglich, M., Jäger, C., Rouillé, G., et al. 2010, *ApJ*, 712, L16
- Valencic, L. A., Clayton, G. C., & Gordon, K. D. 2004, *ApJ*, 616, 912
- Wang, S., & Jiang, B. W. 2014, *ApJL*, 788, L12
- Wang, S., Li, A., & Jiang, B. W. 2014, *P&SS*, 100, 32
- Wang, S., Li, A., & Jiang, B. W. 2015, *ApJ*, 811, 38
- Wang, S., Gao, J., Jiang, B. W., Li, A., & Chen, Y. 2013, *ApJ*, 773, 30
- Wegner, W. 2003, *Astronomische Nachrichten*, 324, 219
- Weingartner, J. C., & Draine, B. T. 2001, *ApJ*, 548, 296 (WD01)
- Witt, A. N. 2014, in *IAU Symp. 297, The Diffuse Interstellar Bands*, ed. J. Cami & N. L. J. Cox (Cambridge: Cambridge Univ. Press), 173
- Witt, A. N., Bohlin, R. C., & Stecher, T. P. 1986, *ApJL*, 305, L23
- Witt, A. N., & Vijh, U. P. 2004, in *ASP Conf. Ser. 309, Astrophysics of Dust*, ed. A.N. Witt, G.C. Clayton, & B.T. Draine (San Francisco: ASP), 115
- Xiang, F. Y., Li, A., & Zhong, J. X. 2017, *ApJ*, 835, 107

Xue, M. Y., Jiang, B. W., Gao, J., et al. 2016, ApJS, 224, 23

Zubko, V., Dwek, E., & Arendt, R. G. 2004, ApJS, 152, 211

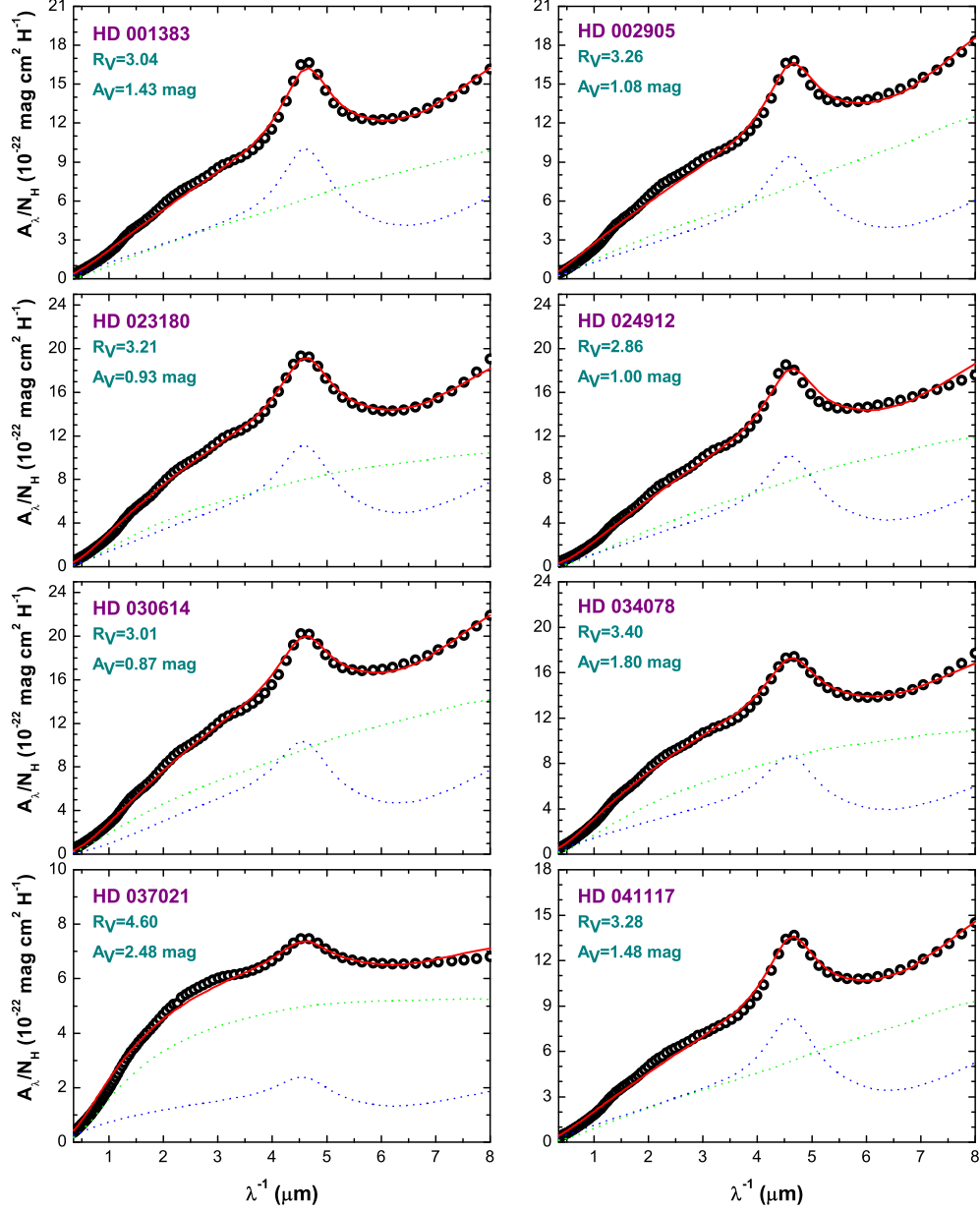


Fig. 1.— Observed and model extinction curves of HD 001383, HD 002905, HD 023180, HD 024912, HD 030614, HD 034078, HD 037021, and HD 041117. The observed extinction curves are represented by the FM90 parametrization at $\lambda^{-1} > 3.3 \mu\text{m}^{-1}$ and by the CCM parametrization at $\lambda^{-1} < 3.3 \mu\text{m}^{-1}$ (open black circle). The solid red line plots the model extinction curve which is a combination of amorphous silicate (dotted green line) and graphite (dashed blue line).

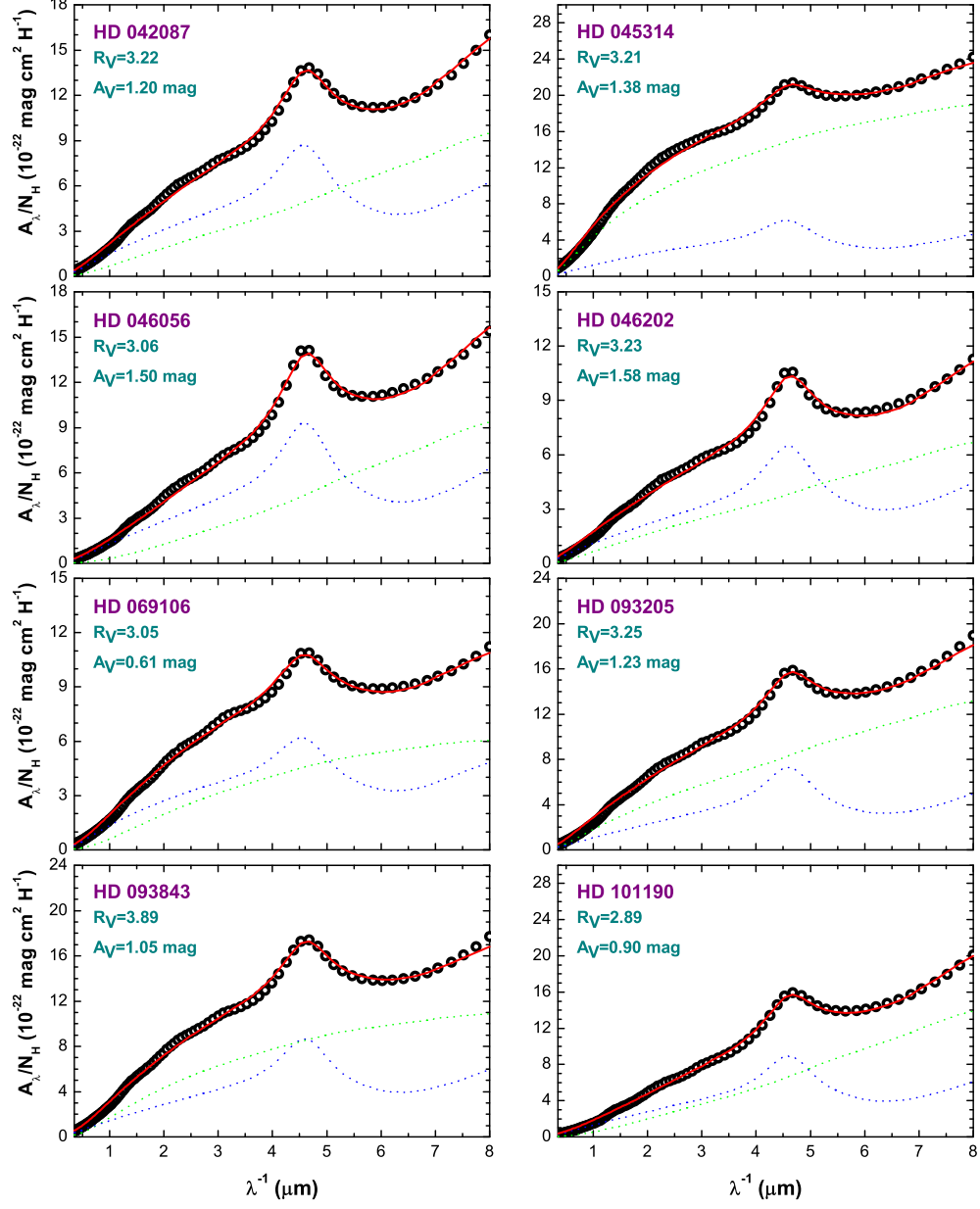


Fig. 2.— Same as Figure 1 but for HD 042087, HD 045314, HD 046056, HD 046202, HD 069106, HD 093205, HD 093843, and HD 101190.

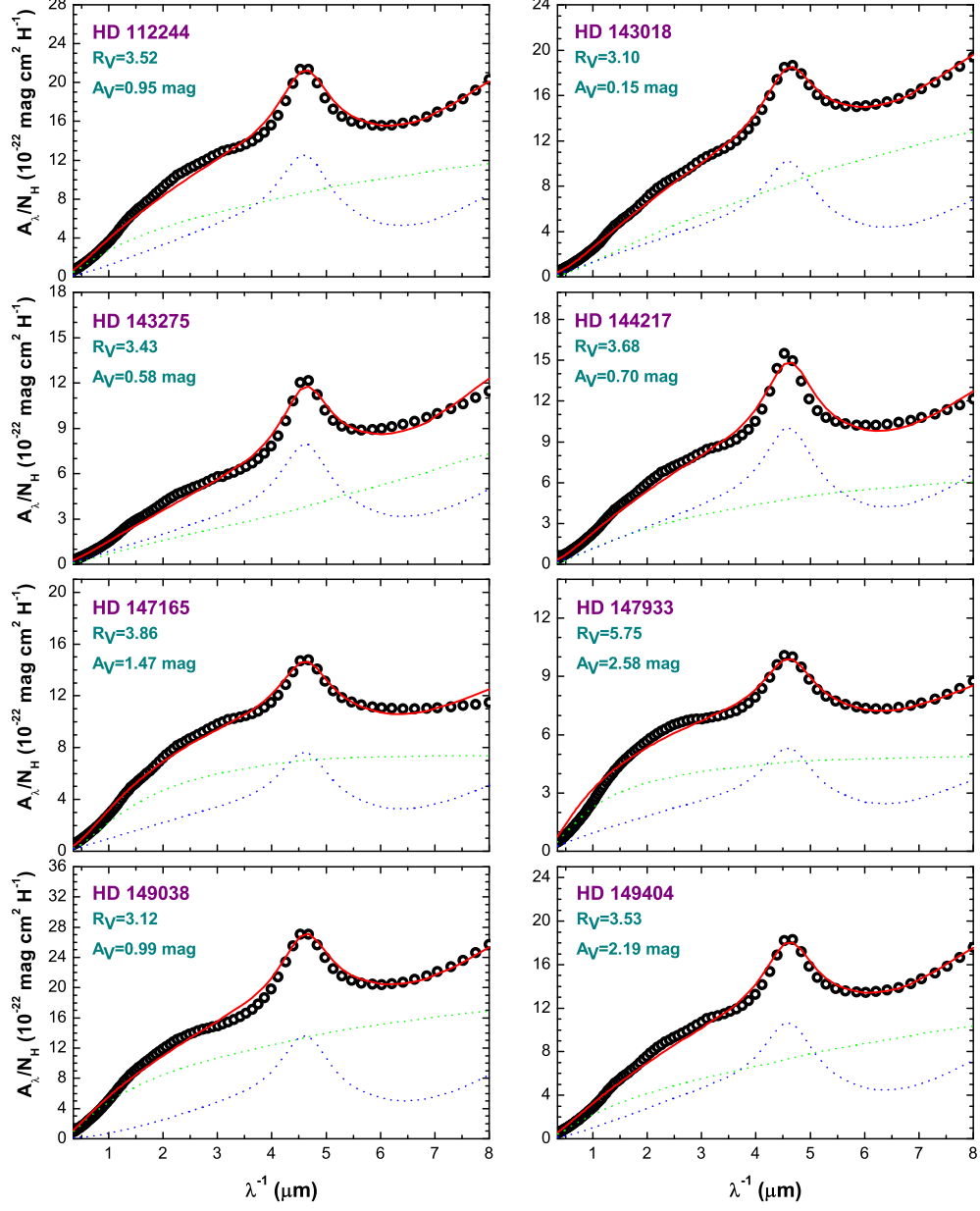


Fig. 3.— Same as Figure 1 but for HD 112244, HD 143018, HD 143275, HD 144217, HD 147165, HD 147933, HD 149038, and HD 149404.

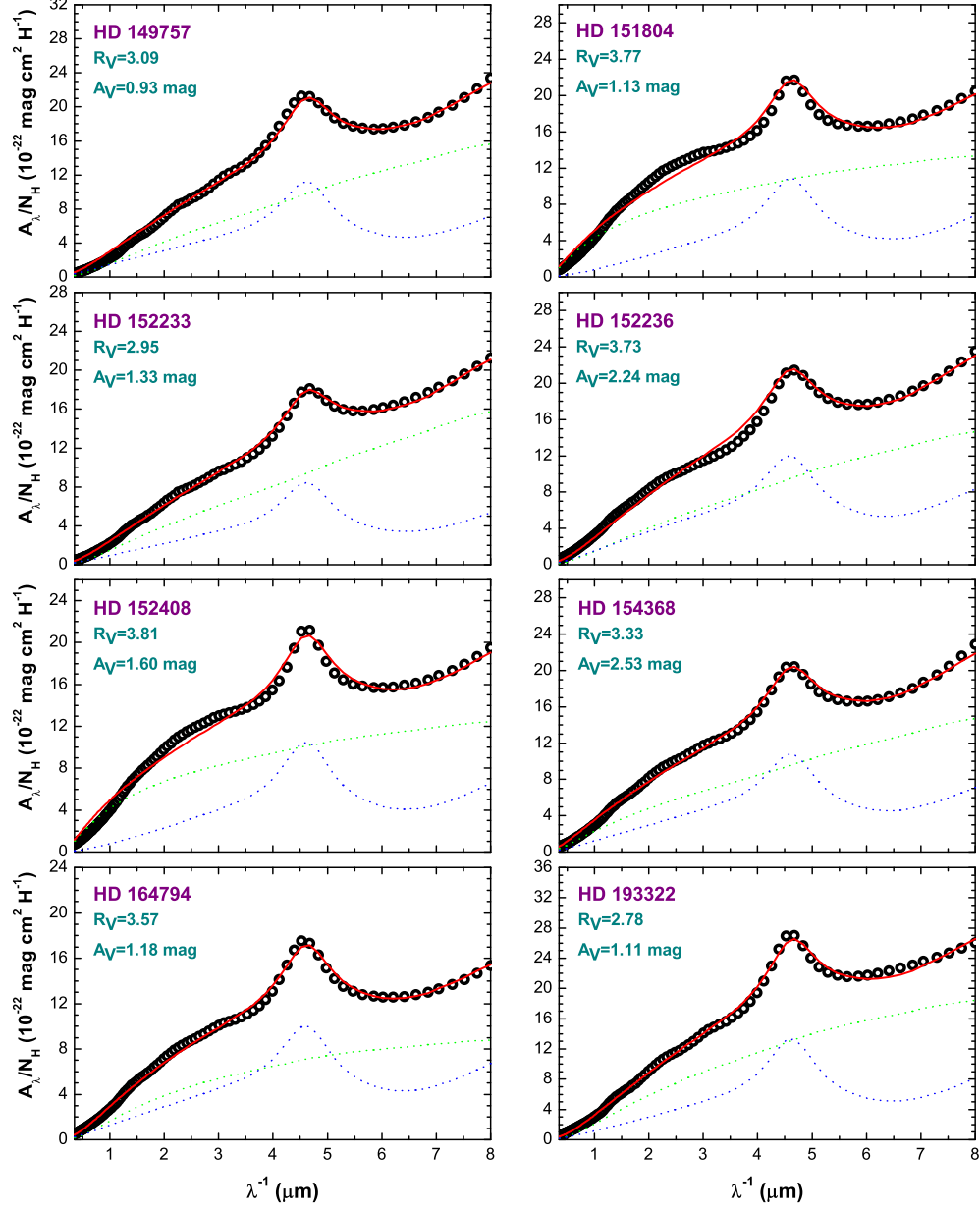


Fig. 4.— Same as Figure 1 but for HD 149757, HD 151804, HD 152233, HD 152236, HD 152408, HD 154368, HD 164794, and HD 193322.

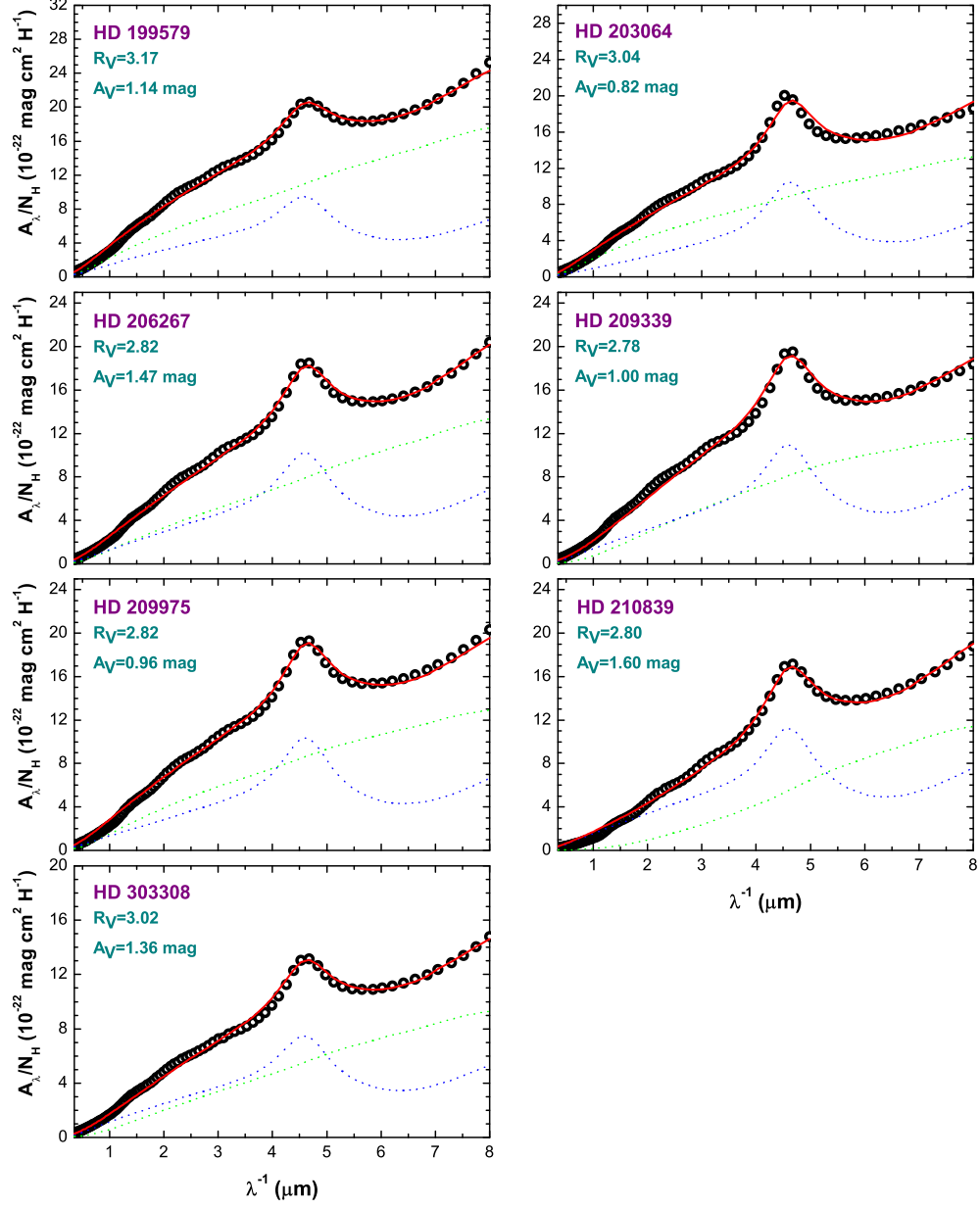


Fig. 5.— Same as Figure 1 but for HD 199579, HD 203064, HD 206267, HD 209339, HD 209975, HD 210839, and HD 303308.

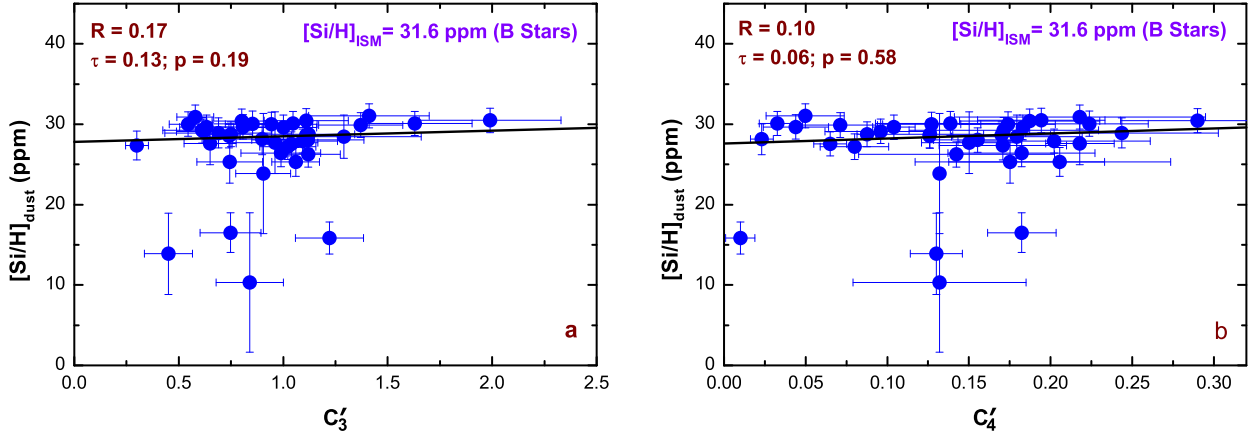


Fig. 6.— Correlation diagrams between the silicon depletion $[\text{Si}/\text{H}]_{\text{dust}}$ and the strength of the 2175 Å extinction bump (c'_3 ; left panel) or the far-UV extinction rise (c'_4 ; right panel), where $[\text{Si}/\text{H}]_{\text{dust}} = [\text{Si}/\text{H}]_{\text{ISM}} - [\text{Si}/\text{H}]_{\text{gas}}$. The interstellar silicon reference abundance $[\text{Si}/\text{H}]_{\text{ISM}}$ is assumed to be that of B stars (Przybilla et al. 2008). The gas-phase silicon abundance $[\text{Si}/\text{H}]_{\text{gas}}$ is taken from Haris et al. (2016). Note that the exact value of the assumed interstellar silicon reference abundance (of proto-Sun or B stars) does not affect the correlation coefficient but the intercept. Also labelled are the Kendall's τ coefficient and the significance level p .

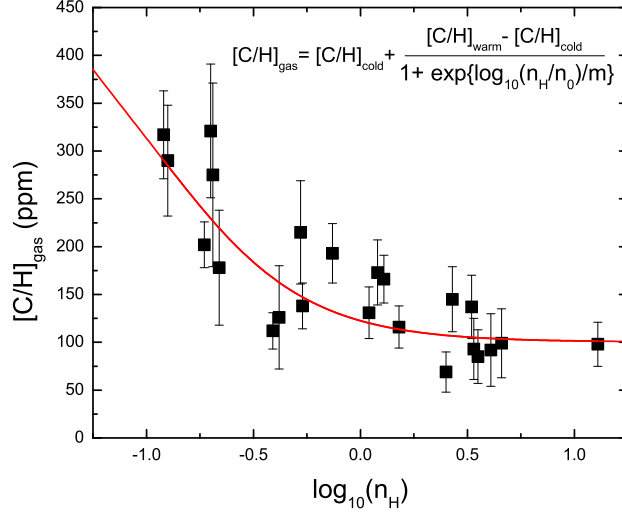


Fig. 7.— Density-dependent gas-phase carbon abundance $[C/H]_{\text{gas}}$ (black squares) fitted by a Boltzmann function (red line) characterized by a set of four parameters: $[C/H]_{\text{warm}} \approx 480 \pm 48$ ppm, $[C/H]_{\text{cold}} \approx 100 \pm 15$ ppm, $\log_{10}(n_0/\text{cm}^{-3}) \approx -0.92 \pm -0.10$, and $m \approx 0.33 \pm 0.12$.

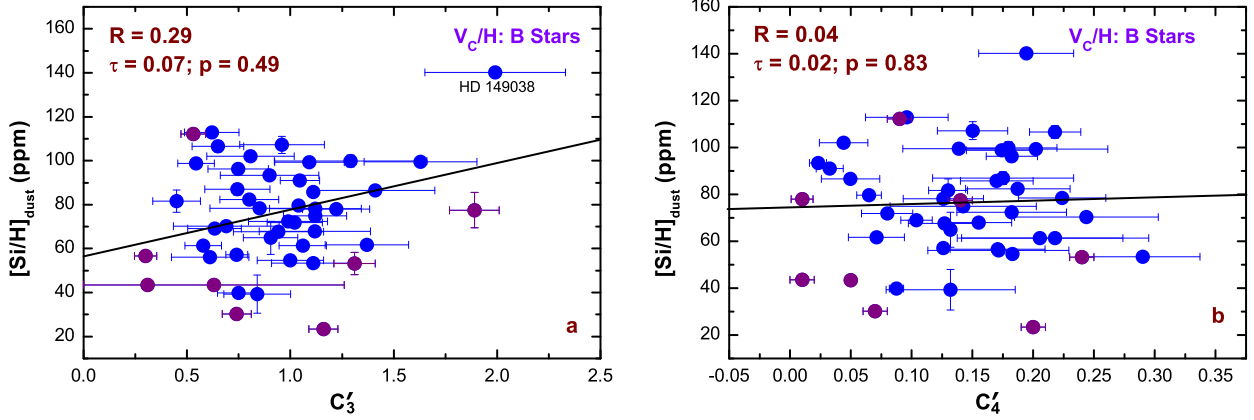


Fig. 8.— Correlation diagrams between $[Si/H]_{\text{dust}}$ and the 2175 Å bump (c'_3 ; left panel) or the far-UV rise (c'_4 ; right panel). The silicon depletion $[Si/H]_{\text{dust}}$ is derived from the Kramers-Kronig relation, with the interstellar carbon reference abundance $[C/H]_{\text{ISM}}$ taken to be that of B stars (Przybilla et al. 2008) and the gas-phase carbon abundance $[C/H]_{\text{gas}}$ derived from the hydrogen number density n_H based on the Boltzmann function (see Figure 7). Similar to Figure 6, the exact value of the assumed interstellar C/H abundance (of proto-Sun or B stars) does not affect the correlation coefficient but the intercept.

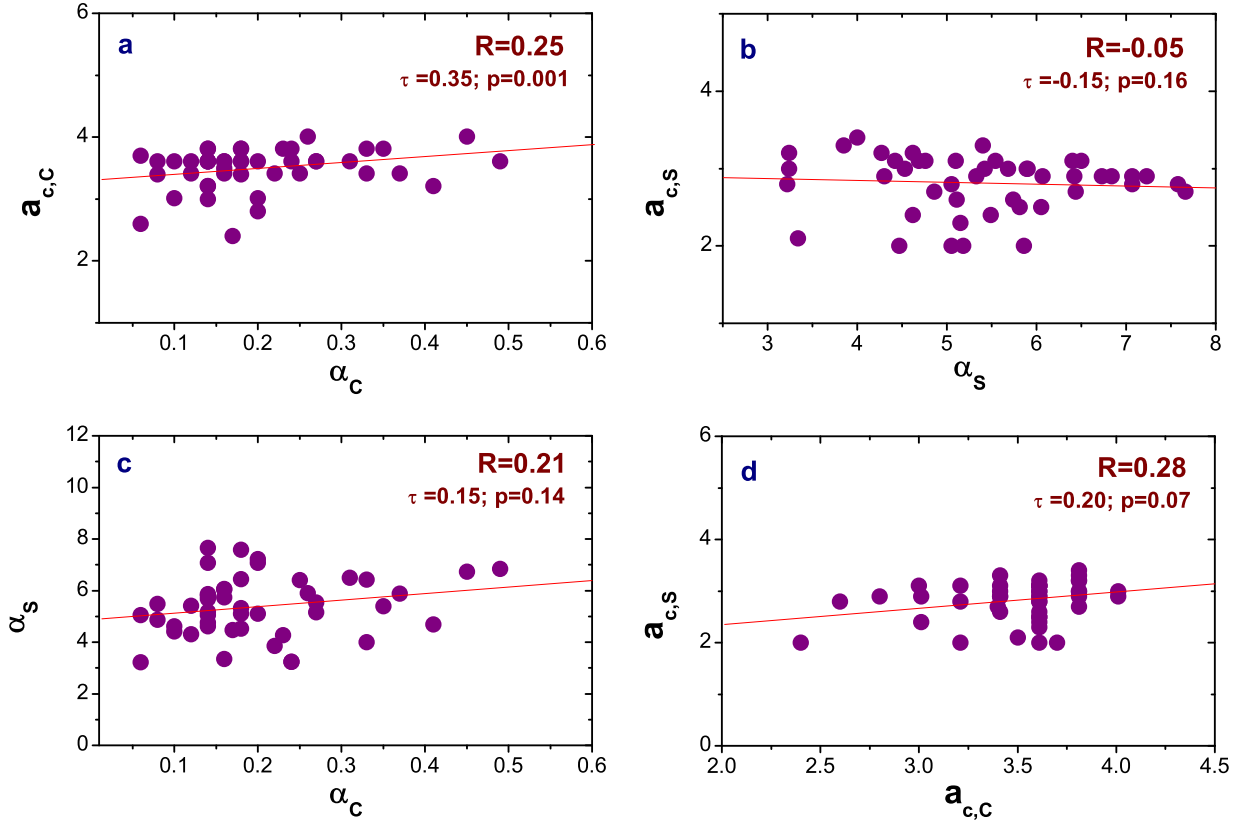


Fig. 9.— Interrelations among the model parameters $a_{c,S}$ – the exponential cutoff size of silicate dust, $a_{c,C}$ – the exponential cutoff size of graphite, α_S – the size distribution power index of silicate dust, and α_C – the size distribution power index of graphite.

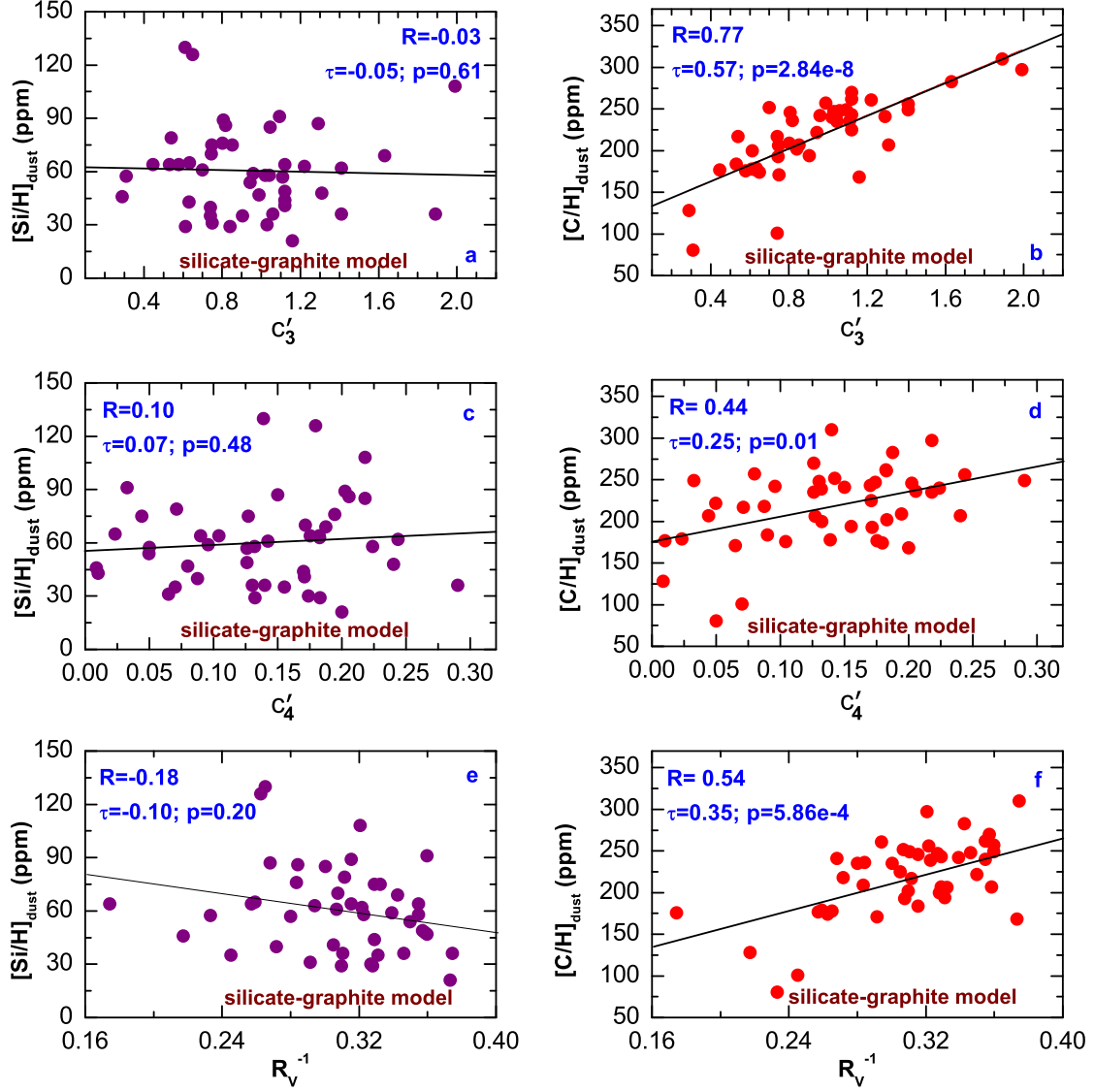


Fig. 10.— Upper panel: Correlation diagrams between the 2175 Å bump (c'_3) and the silicon depletion $[\text{Si}/\text{H}]_{\text{dust}}$ (a) or the carbon depletion $[\text{C}/\text{H}]_{\text{dust}}$ (b) derived from fitting the extinction curve of each sightline with a mixture of amorphous silicate dust and graphite dust. Middle panel: The correlations between the far-UV nonlinear extinction rise (c'_4) and $[\text{Si}/\text{H}]_{\text{dust}}$ (c) or $[\text{C}/\text{H}]_{\text{dust}}$ (d). Lower panel: The correlations between R_V^{-1} and $[\text{Si}/\text{H}]_{\text{dust}}$ (e) or $[\text{C}/\text{H}]_{\text{dust}}$ (f).

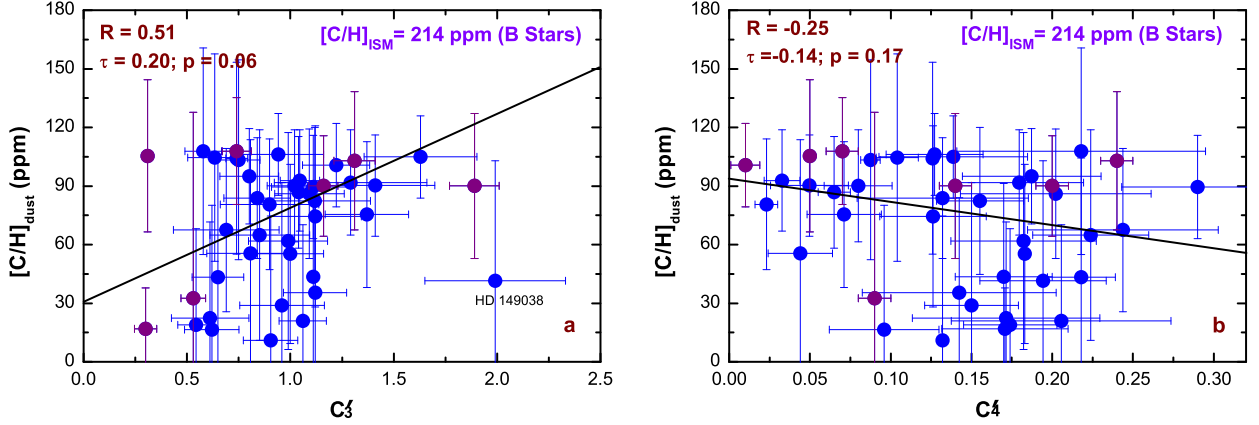


Fig. 11.— Correlation diagrams between the carbon depletion $[C/H]_{\text{dust}}$ and the strength of the 2175 Å extinction bump (c'_3 ; left panel) or the far-UV extinction rise (c'_4 ; right panel), where $[C/H]_{\text{dust}} = [C/H]_{\text{ISM}} - [C/H]_{\text{gas}}$. The interstellar carbon reference abundance $[C/H]_{\text{ISM}}$ is assumed to be that of B stars (Przybilla et al. 2008). The gas-phase carbon abundance $[C/H]_{\text{gas}}$ is derived from n_{H} based on the Boltzmann function (see Figure 7). Similar to Figure 6, the exact value of the assumed interstellar C/H abundance does not affect the correlation coefficient but the intercept.

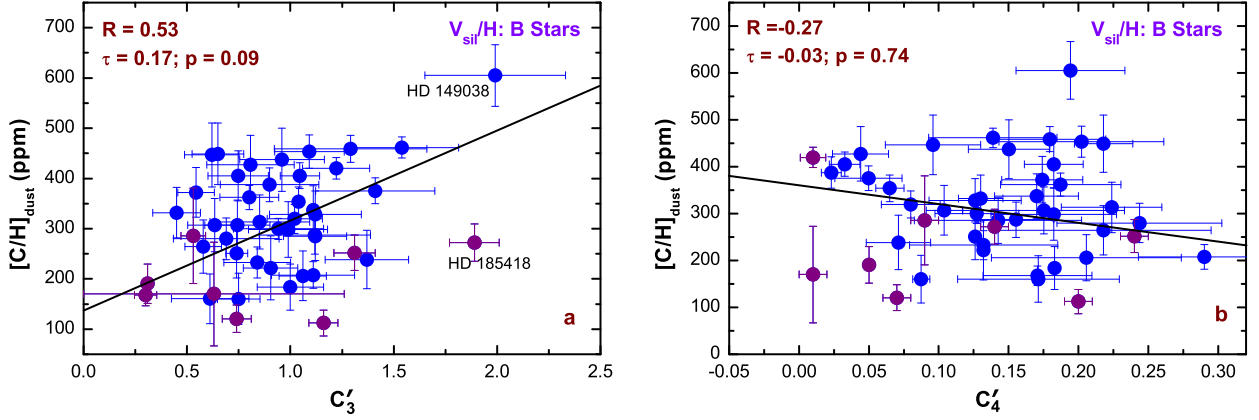


Fig. 12.— Correlation diagrams between $[C/H]_{\text{dust}}$ and the 2175 Å bump (c'_3 ; left panel) or the far-UV extinction rise (c'_4 ; right panel). The carbon depletion $[C/H]_{\text{dust}}$ is derived from the Kramers-Kronig relation, with the interstellar Fe, Mg, and Si reference abundances taken to be that of B stars (Przybilla et al. 2008) and the gas-phase silicon abundance $[Si/H]_{\text{gas}}$ taken from Haris et al. (2016). Similar to Figure 6, the exact values of the assumed interstellar Fe/H, Mg/H and Si/H abundances do not affect the correlation coefficient but the intercept.

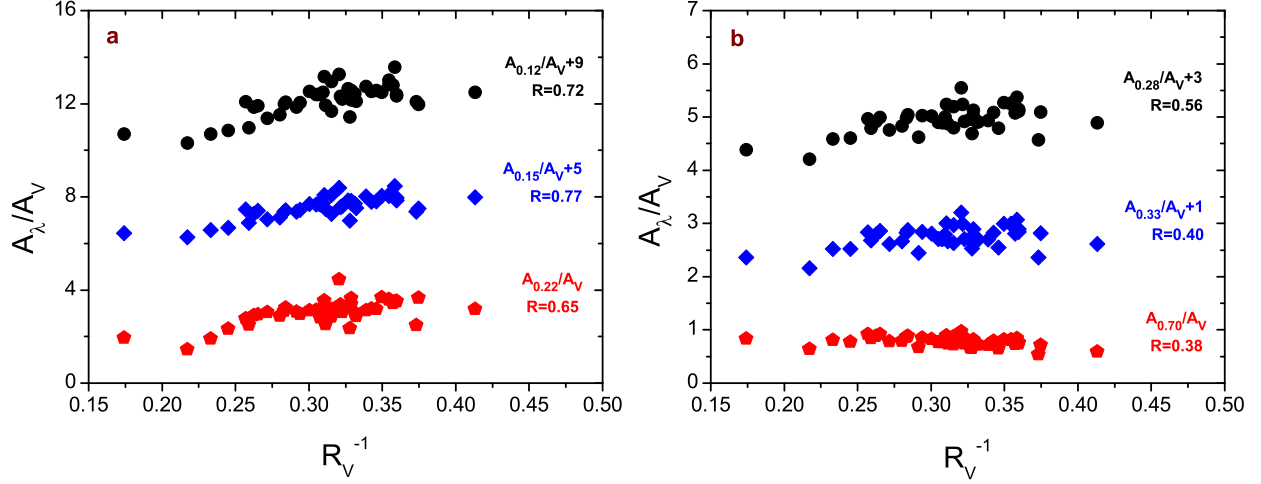


Fig. 13.— The extinction ratio A_λ/A_V plotted against R_V^{-1} at selected wavelengths. The subscripts refer to the wavelength (e.g., $A_{0.12}$ refers to the extinction at $\lambda = 0.12 \mu\text{m}$). The data for $\lambda = 0.12, 0.15, 0.28, 0.33 \mu\text{m}$ have been shifted vertically by the amount indicated in order to separate them.

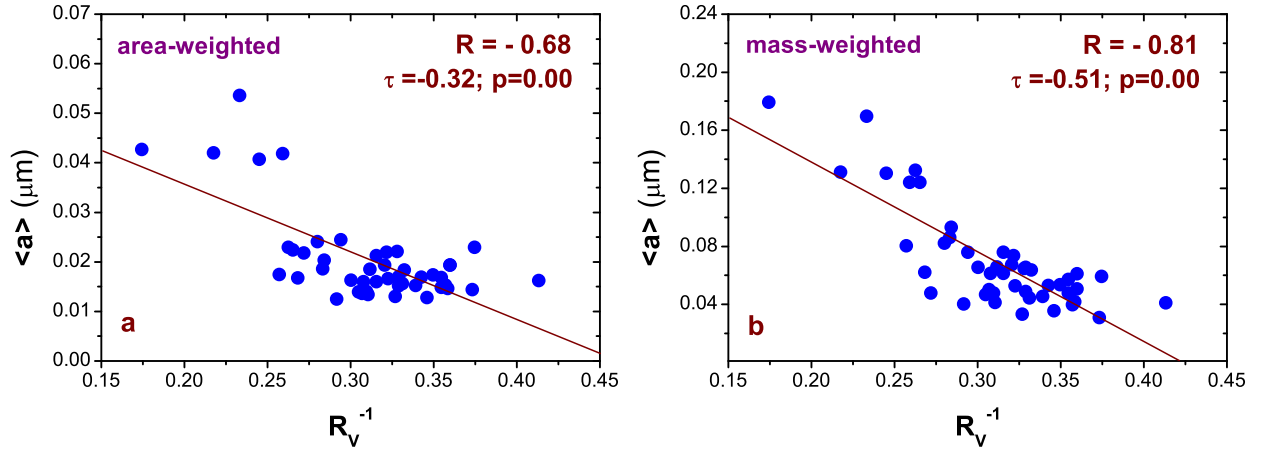


Fig. 14.— Area-weighted (a) and mass-weighted (b) mean grain sizes vs. R_V^{-1} .

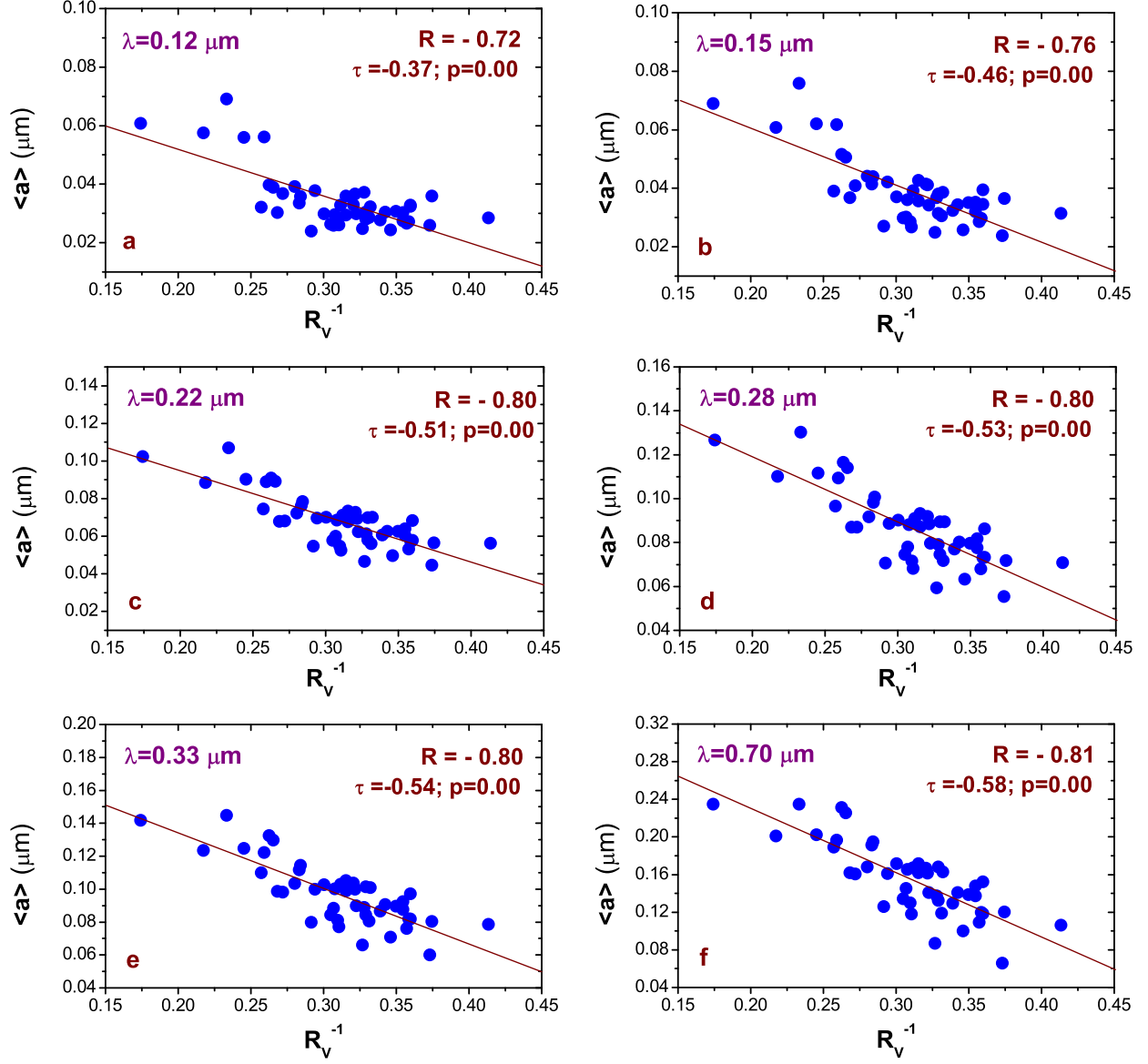


Fig. 15.— Extinction-weighted mean grain sizes vs. R_V^{-1} . The weighting extinction cross sections $C_{\text{ext}}(a, \lambda)$ are taken to be that at $\lambda = 0.12 \mu\text{m}$ (a), $0.15 \mu\text{m}$ (b), $0.22 \mu\text{m}$ (c), $0.28 \mu\text{m}$ (d), $0.33 \mu\text{m}$ (e), and $0.70 \mu\text{m}$ (f).

Table 1. Extinction Parameters and the Silicon and Carbon Depletions Required to Account for the Observed Extinction

Star	N_{H}^a	$\log_{10}(n_{\text{H}})^b$	R_V	A_V	c'_1	c'_2	c'_3	c'_4	x_0	γ	A_{int}^c	Proto-Sun ^d				B Stars ^e			
HD		(cm ⁻³)		(mag)					(μm ⁻¹)	(μm ⁻¹)		$V_{\text{sil}}/\text{H}^f$	$[\text{Si}/\text{H}]_{\text{dust}}^g$	V_{C}/H^h	$[\text{C}/\text{H}]_{\text{dust}}^i$	$V_{\text{sil}}/\text{H}^f$	$[\text{Si}/\text{H}]_{\text{dust}}^g$	V_{C}/H^h	$[\text{C}/\text{H}]_{\text{dust}}^i$
001383 ¹	3.16 ^{+0.64} _{-0.53}	-0.45	3.04±0.15 ²	1.43±0.14	1.13±0.31	0.21±0.02	1.13±0.15	0.17±0.03	4.60±0.01	0.91±0.03	1.50	4.85E-27	59±2	2.12E-27	238±54	6.11E-27	75±2	2.54E-27	285±49
002905 ¹	2.00	-0.22	3.26±0.20 ⁵	1.08±0.12	1.11±0.80	0.26±0.09	0.69±0.26	0.14±0.06	4.60±0.02	0.82±0.03	1.53	4.47E-27	55±2	2.07E-27	233±48	5.73E-27	70±2	2.49E-27	280±42
023180 ¹	1.62	0.065	3.11±0.39 ¹	0.93±0.17	1.49±0.53	0.10±0.02	1.41±0.29	0.24±0.06	4.57±0.02	1.11±0.04	1.91	5.80E-27	71±2	2.92E-27	329±35	7.06E-27	87±2	3.34E-27	375±26
024912 ¹	1.98 ^{+0.54} _{-0.54}	0.75	2.86±0.51 ¹	1.00±0.21	1.19±0.73	0.27±0.05	0.94±0.22	0.05±0.02	4.54±0.02	0.85±0.03	1.62	4.26E-27	52±2	2.25E-27	253±31	5.52E-27	68±2	2.66E-27	300±21
030614 ¹	1.23	-0.64	3.01±0.33 ¹	0.87±0.15	1.10±0.29	0.20±0.03	0.75±0.15	0.13±0.03	4.57±0.01	0.90±0.03	1.75	6.60E-27	81±3	3.19E-27	358±55	7.86E-27	96±2	3.60E-27	405±50
034078 ¹	3.10	0.35	3.40±0.22 ¹	1.80±0.18	1.37±0.20	0.14±0.02	1.22±0.16	0.18±0.02	4.60±0.00	1.11±0.03	1.79	5.10E-27	63±2	3.32E-27	373±32	6.36E-27	78±2	3.73E-27	420±21
037021 ¹	4.79 ^{+1.52} _{-1.16}	0.61	4.60±0.12 ⁶	2.48±0.06	1.08±1.06	0.03±0.01	0.30±0.05	0.01±0.01	4.58±0.05	1.08±0.04	1.10	3.36E-27	41±2	1.07E-27	121±31	4.62E-27	57±2	1.49E-27	168±21
041117 ¹	3.47 ^{+1.43} _{-0.90}	0.05	3.28±0.14 ⁵	1.48±0.06	1.04±0.36	0.23±0.03	1.30±0.20	0.23±0.04	4.61±0.01	0.99±0.03	1.30	3.10E-27	38±2	1.43E-27	161±35	4.36E-27	53±2	1.85E-27	208±27
042087 ¹	3.09 ^{+0.71} _{-0.58}	-0.14	3.22 ⁷	1.19±0.13	1.08±0.69	0.26±0.04	1.38±0.20	0.29±0.05	4.61±0.00	1.07±0.02	1.40	3.77E-27	46±2	1.70E-27	192±63	5.03E-27	62±2	2.12E-27	238±58
045314 ¹	1.91	-0.53	3.21±0.14 ⁵	1.38±0.14	1.09±0.22	0.20±0.02	0.54±0.09	0.07±0.02	4.59±0.02	0.90±0.03	1.88	6.80E-27	83±2	2.89E-27	325±55	8.06E-27	99±2	3.31E-27	372±49
046056 ¹	3.39 ^{+0.98} _{-0.76}	-0.32	3.06±0.11 ⁵	1.50±0.13	0.79±0.34	0.29±0.03	1.04±0.16	0.18±0.03	4.58±0.01	0.91±0.03	1.20	3.20E-27	39±2	1.22E-27	137±51	4.46E-27	55±2	1.64E-27	184±46
046202 ³	4.79 ^{+1.67} _{-1.16}	-0.04	3.23±0.14 ⁵	1.55±0.15	1.03	0.23	0.84	0.18	4.59	0.86	1.02	1.94E-27	24±9	1.65E-27	186±39	3.20E-27	39±9	2.07E-27	233±31
069106 ¹	1.32 ^{+0.19} _{-0.14}	-0.52	3.05±0.44 ¹	0.61±0.15	1.27±0.65	0.10±0.03	0.61±0.19	0.13±0.05	4.59±0.02	0.96±0.03	1.11	3.32E-27	41±2	1.01E-27	114±55	4.58E-27	56±2	1.43E-27	161±49
093205 ¹	2.24	-0.66	3.25±0.24 ¹	1.24±0.16	0.93±0.51	0.25±0.03	0.74±0.16	0.17±0.06	4.61±0.04	0.96±0.03	1.56	5.83E-27	71±3	2.31E-27	260±55	7.09E-27	87±3	2.73E-27	307±50
093843 ¹	2.24 ^{+0.45} _{-0.38}	-0.68	3.89±0.41 ¹	1.05±0.22	1.37±0.50	0.15±0.03	0.45±0.11	0.18±0.06	4.57±0.03	0.78±0.03	1.44	5.40E-27	66±5	2.54E-27	285±55	6.66E-27	82±5	2.95E-27	332±50
101190 ²	1.95	-0.52	2.89±0.39 ²	0.90±0.13	0.44±0.09	0.34±0.02	1.06±0.11	0.13±0.02	4.59±0.05	0.93±0.02	1.20	3.74E-27	46±2	1.42E-27	159±55	5.00E-27	61±2	1.83E-27	206±49
112244 ¹	1.48	-0.08	3.52±0.16 ⁵	0.95±0.32	1.50±0.49	0.11±0.03	0.89±0.24	0.21±0.07	4.59±0.01	0.85±0.03	1.90	6.35E-27	78±2	3.03E-27	341±41	7.61E-27	93±2	3.45E-27	388±33
143018 ⁵	0.56 ^{+0.05} _{-0.05}	0.005	3.10 ⁴	0.34	0.98	0.23	1.04	0.13	4.60	0.99	1.77	5.23E-27	64±2	2.73E-27	307±37	6.49E-27	80±2	3.15E-27	354±29
143275 ⁵	1.45 ^{+0.28} _{-0.28}	0.49	3.43±0.04 ⁴	0.58±0.01	0.62±0.06	0.25±0.01	0.76±0.10	0.07±0.01	4.56±0.01	0.77±0.06	1.10	1.99E-27	24±2	1.01E-27	113±56	3.25E-27	40±2	1.43E-27	160±51
144217 ⁵	1.37 ^{+0.12} _{-0.12}	0.55	3.68±0.03 ⁴	0.70±0.01	1.29±0.04	0.10±0.01	0.74±0.05	0.09±0.01	4.50±0.01	0.66±0.03	1.42	3.40E-27	42±2	1.81E-27	204±54	4.66E-27	57±2	2.23E-27	251±49
147165 ¹	2.51 ^{+0.51} _{-0.42}	0.58	3.86±0.52 ¹	1.47±0.23	1.56±0.30	0.04±0.01	0.63±0.13	0.02±0.01	4.61±0.01	0.89±0.03	1.64	4.37E-27	54±2	2.31E-27	260±58	5.63E-27	69±2	2.73E-27	307±53
147933 ¹	5.01 ^{+0.80} _{-0.80}	1.13	5.74±0.40 ¹	2.58±0.34	1.23±0.17	0.02±0.01	0.58±0.09	0.10±0.01	4.58±0.01	0.95±0.03	1.51	3.74E-27	46±2	1.93E-27	217±58	5.00E-27	61±2	2.35E-27	264±53
149038 ¹	1.32	-0.41	3.12±0.15 ⁵	1.00±0.05	1.29±0.26	0.29±0.07	1.99±0.53	0.22±0.08	4.58±0.01	0.99±0.03	2.72	1.02E-26	125±2	4.96E-27	558±66	1.14E-26	140±2	5.38E-27	605±61
149404 ¹	3.72	0.17	3.53±0.38 ¹	2.19±0.32	1.45±0.31	0.12±0.02	0.80±0.14	0.19±0.04	4.60±0.01	0.86±0.03	1.85	5.46E-27	67±2	2.80E-27	315±34	6.72E-27	82±2	3.22E-27	362±24
149757 ¹	1.40 ^{+0.03} _{-0.03}	0.61	3.09 ⁸	0.99±0.12	1.00±0.26	0.24±0.03	1.55±0.26	0.18±0.04	4.55±0.01	1.19±0.04	2.20	6.86E-27	84±2	3.69E-27	415±31	8.12E-27	100±2	4.10E-27	461±21
151804 ¹	1.68	-0.54	3.77±0.16 ⁵	1.13±0.12	1.45±0.38	0.13±0.03	0.62±0.13	0.14±0.05	4.60±0.02	0.76±0.02	2.13	7.95E-27	97±2	3.56E-27	400±68	9.21E-27	113±2	3.97E-27	447±64
152233 ¹	2.34	-0.48	2.95±0.29 ¹	1.33±0.24	0.54±0.15	0.36±0.05	0.96±0.21	0.10±0.03	4.61±0.03	0.99±0.03	2.07	7.48E-27	92±4	3.47E-27	390±67	8.75E-27	107±4	3.89E-27	437±63
152236 ¹	6.92 ^{+1.99} _{-1.55}	0.09	3.73±0.39 ¹	2.24±0.26	0.76±0.66	0.26±0.05	1.29±0.37	0.15±0.03	4.61±0.02	1.10±0.09	2.16	6.89E-27	84±3	3.66E-27	412±36	8.15E-27	100±3	4.08E-27	459±27
152408 ¹	2.34	-0.40	3.81±0.13 ⁵	1.60±0.20	1.45±0.24	0.11±0.02	0.65±0.12	0.18±0.04	4.58±0.01	0.79±0.03	2.11	7.43E-27	91±3	3.58E-27	402±65	8.70E-27	107±3	3.99E-27	449±61
154368 ¹	3.89 ^{+0.47} _{-0.42}	0.12	3.33±0.15 ¹	2.53±0.20	1.09±0.10	0.22±0.01	1.05±0.09	0.22±0.02	4.58±0.00	1.00±0.02	2.00	6.16E-27	75±2	3.19E-27	359±35	7.42E-27	91±2	3.61E-27	405±26
164794 ³	1.95	-0.40	3.57±0.17 ⁵	1.18±0.06	1.31	0.10	1.11	0.13	4.56	0.99	1.73	5.74E-27	70±2	2.58E-27	290±53	7.00E-27	86±2	3.00E-27	337±48
193322 ¹	1.45	-0.007	2.78±0.26 ¹	1.11±0.15	0.91±0.28	0.30±0.04	1.09±0.17	0.03±0.01	4.58±0.01	0.92±0.03	2.13	6.84E-27	84±2	3.61E-27	406±41	8.11E-27	99±2	4.03E-27	453±33
199579 ¹	1.78 ^{+0.31} _{-0.26}	-0.32	3.17±0.69 ¹	1.14±0.28	1.10±0.55	0.28±0.06	0.81±0.21	0.20±0.06	4.59±0.01	0.99±0.03	2.07	7.06E-27	87±2	3.38E-27	380±63	8.32E-27	102±2	3.80E-27	427±58

Table 1—Continued

Star	N_{H}^a	$\log_{10}(n_{\text{H}})^b$	R_V	A_V	c'_1	c'_2	c'_3	c'_4	x_0	γ	A_{int}^c	Proto-Sun ^d				B Stars ^e			
HD		(cm ⁻³)		(mag)					(μm ⁻¹)	(μm ⁻¹)		$V_{\text{sil}}/\text{H}^f$	$[\text{Si}/\text{H}]_{\text{dust}}^g$	V_{C}/H^h	$[\text{C}/\text{H}]_{\text{dust}}^i$	$V_{\text{sil}}/\text{H}^f$	$[\text{Si}/\text{H}]_{\text{dust}}^g$	V_{C}/H^h	$[\text{C}/\text{H}]_{\text{dust}}^i$
203064 ¹	1.39	-0.25	3.04±0.36 ¹	0.82±0.16	1.00±0.21	0.25±0.05	0.85±0.24	0.04±0.02	4.54±0.02	0.82±0.03	1.67	5.13E-27	63±2	2.37E-27	266±59	6.40E-27	78±2	2.79E-27	313±54
206267 ¹	2.88 ^{+0.28} _{-0.25}	0.06	2.82±0.16 ¹	1.47±0.14	1.17±0.36	0.27±0.02	1.02±0.13	0.22±0.04	4.59±0.01	0.91±0.03	1.64	4.60E-27	56±2	2.42E-27	273±37	5.86E-27	72±2	2.84E-27	319±29
209339 ¹	1.82 ^{+0.27} _{-0.23}	-0.27	2.78±0.34 ¹	1.00±0.23	1.16±0.30	0.24±0.04	0.99±0.19	0.08±0.02	4.60±0.01	0.88±0.03	1.55	4.65E-27	57±2	2.24E-27	251±60	5.91E-27	72±2	2.65E-27	298±55
209975 ¹	1.80	-0.15	2.82±0.38 ¹	0.96±0.17	1.17±0.41	0.26±0.04	1.12±0.22	0.18±0.04	4.59±0.01	0.94±0.03	1.70	5.12E-27	63±2	2.50E-27	281±52	6.38E-27	78±2	2.92E-27	328±46
210839 ¹	2.95 ^{+0.28} _{-0.26}	-0.06	2.80 ⁹	1.60±0.11	0.76±0.56	0.33±0.06	1.12±0.27	0.13±0.03	4.60±0.02	0.96±0.06	1.54	4.28E-27	52±2	2.14E-27	240±44	5.54E-27	68±2	2.55E-27	287±38
303308 ¹	3.16	-0.57	3.02±0.21 ¹	1.36±0.18	0.87±0.21	0.26±0.03	0.90±0.13	0.16±0.03	4.59±0.01	0.95±0.03	1.23	4.03E-27	49±8	1.56E-27	175±68	5.30E-27	175±7	1.97E-27	222±64
027778 ²	2.29±1.20	0.53	2.79±0.38 ²	1.09±0.03	0.87±0.71	0.32±0.01	1.31±0.10	0.24±0.01	4.59±0.04	1.21±0.03	1.39	3.08E-27	38±4	1.82E-27	205±42	4.34E-27	53±5	2.24E-27	252±35
037061 ²	5.37±1.23	0.66	4.29±0.21 ²	2.40±0.21	1.54±0.00	0.00±0.00	0.31±0.00	0.05±0.00	4.57±0.00	0.90±0.00	1.19	2.28E-27	28±2	1.28E-27	144±46	3.55E-27	43±2	1.69E-27	190±39
116852 ¹	1.05±1.20	-1.15	2.42±0.37 ¹	0.51±0.12	0.52±0.25	0.38±0.10	0.63±0.17	0.01±0.01	4.55±0.04	0.78±0.07	1.13	2.29E-27	28±2	1.09E-27	123±106	3.55E-27	44±2	1.51E-27	170±103
122879 ²	2.19±1.26	-0.47	3.17±0.20 ²	1.41±0.04	1.15±0.08	0.15±0.02	0.53±0.06	0.09±0.01	4.57±0.04	0.74±0.02	1.50	7.89E-27	97±2	2.12E-27	239±98	9.15E-27	112±2	2.54E-27	286±95
147888 ²	5.89±1.20	1.11	4.08±0.18 ²	1.97±0.03	1.43±0.05	0.03±0.01	0.74±0.07	0.07±0.01	4.58±0.03	0.94±0.02	0.95	1.21E-27	15±2	0.66E-27	74±36	2.47E-27	30±2	1.07E-27	121±27
185418 ²	2.57±1.17	0.08	2.67±0.20 ²	1.39±0.04	1.37±0.09	0.16±0.02	1.89±0.12	0.14±0.01	4.59±0.03	1.03±0.02	1.55	5.06E-27	62±6	2.00E-27	225±44	6.32E-27	77±8	2.42E-27	272±37
207198 ²	4.79±1.23	0.40	2.68±0.11 ²	1.54±0.03	0.73±0.05	0.35±0.01	1.16±0.07	0.20±0.01	4.62±0.03	1.04±0.02	0.93	0.65E-27	8.0±2	0.58E-27	65±35	1.91E-27	24±2	1.00E-27	112±26

^a Taken from Gudennavar et al. (2012) along with upper and lower uncertainty (in unit of 10²¹ cm⁻² H)^b Taken from Haris et al. (2016)^c The wavelength-integrated extinction $A_{\text{int}} \equiv \int_{912 \text{ \AA}}^{10^3 \mu\text{m}} A_{\lambda}/N_{\text{H}} d\lambda$ (in unit of 10⁻²⁵ mag cm³ H⁻¹)^d The interstellar Si, Mg and Fe abundances are taken to be that of proto-Sun (Lodders 2003) for which the total silicate volume per H atom is $V_{\text{sil}}/\text{H} \approx 3.17 \times 10^{-27} \text{ cm}^3 \text{ H}^{-1}$.^e The interstellar Si, Mg and Fe abundances are taken to be that of unevolved early B stars (Prybylla et al. 2008) for which $V_{\text{sil}}/\text{H} \approx 2.52 \times 10^{-27} \text{ cm}^3 \text{ H}^{-1}$.^f The total volume of silicon dust per H atom (in unit of cm³ H⁻¹) required to account for the observed extinction.^g The silicon depletion $[\text{Si}/\text{H}]_{\text{dust}}$ (in unit of ppm) required to account for the observed extinction.^h The total volume of carbon dust per H atom (in unit of cm³ H⁻¹) required to account for the observed extinction.ⁱ The carbon depletion $[\text{C}/\text{H}]_{\text{dust}}$ (in unit of ppm) required to account for the observed extinction.

(1) Valencic et al. (2004); (2) Gordon et al. (2009); (3) Jenniskens & Greenberg (1993); (4) Lewis et al. (2005); (5) Wegner et al. (2003); (6) Sofia et al. (2004); (7) Gnaniński & Sikorski (1999); (8) Cardelli et al. (1989); (9) Rachford et al. (2008).

Table 2. Model Parameters for Fitting the UV/Optical/Near-IR Extinction with A Mixture of Silicate/Graphite Dust

Star	A_V/N_H (10^{-22} mag cm 2 H $^{-1}$)	α_S	$a_{c,S}$ (μ m)	α_C	$a_{c,C}$ (μ m)	χ^2/dof	[C/H] $_{\text{gas}}$ (ppm)	[C/H] $_{\text{dust}}$ (ppm)	[Si/H] $_{\text{gas}}^2$ (ppm)	[Si/H] $_{\text{dust}}$ (ppm)
HD 001383	4.53	-3.0	0.18	-3.81	0.55	0.20	173 \pm 46 ¹	243	5.36 \pm 0.49	44
HD 002905	5.40	-3.3	0.35	-3.81	0.80	0.53	141 \pm 39 ¹	252	2.68 \pm 1.10	61
HD 023180	5.74	-2.6	0.16	-3.41	0.15	0.13	119 \pm 21 ¹	256	0.56 \pm 0.03	62
HD 024912	5.05	-2.8	0.14	-3.61	0.20	0.20	103 \pm 15 ¹	222	1.61 \pm 0.03	54
HD 030614	7.07	-2.9	0.20	-2.80	0.05	0.27	214 \pm 48 ¹	206	15.10 \pm 1.95	75
HD 034078	5.81	-2.5	0.14	-3.61	0.50	0.14	108 \pm 15 ¹	261	15.75 \pm 1.35	63
HD 037021	5.18	-2.0	0.14	-3.21	0.50	0.28	192 \pm 15 ⁴	128	4.24 \pm 0.95	46
HD 041117	4.27	-3.2	0.23	-3.81	0.90	0.45	119 \pm 22 ¹	225	1.14 \pm 0.08	41
HD 042087	3.85	-3.3	0.22	-3.41	0.25	0.24	134 \pm 34 ¹	249	1.69 \pm 0.40	36
HD 045314	7.23	-2.9	0.20	-3.01	0.10	0.15	190 \pm 47 ¹	217	1.58 \pm 0.22	79
HD 046056	4.42	-3.1	0.10	-3.61	0.30	0.30	154 \pm 43 ¹	247	1.99 \pm 0.40	30
HD 046202	3.24	-3.2	0.24	-3.61	0.55	0.57	125 \pm 27 ¹	202	21.30 \pm 8.55	29
HD 069106	4.62	-2.4	0.10	-3.01	0.15	0.17	187 \pm 47 ¹	200	2.33 \pm 0.54	29
HD 093205	5.54	-3.1	0.27	-3.61	0.35	0.39	219 \pm 48 ¹	193	6.29 \pm 2.19	70
HD 093843	4.69	-3.1	0.41	-3.21	0.15	0.47	225 \pm 48 ¹	177	17.72 \pm 4.82	64
HD 101190	4.62	-3.2	0.14	-3.81	0.85	0.57	188 \pm 47 ¹	248	6.29 \pm 1.01	36
HD 112244	6.42	-2.9	0.33	-3.41	0.10	0.36	128 \pm 30 ¹	236	3.46 \pm 1.20	86
HD 143018	6.07	-2.9	0.16	-3.61	0.25	0.18	122 \pm 24 ¹	239	4.04 \pm 0.07	58
HD 143275	4.00	-3.4	0.33	-3.81	0.38	0.51	106 \pm 49 ¹	171	2.83 \pm 0.32	31
HD 144217	5.11	-2.6	0.18	-3.61	0.20	0.35	105 \pm 47 ¹	217	3.04 \pm 0.07	40
HD 147165	5.86	-2.0	0.14	-3.61	0.25	0.18	104 \pm 51 ¹	179	1.96 \pm 0.17	65
HD 147933	5.15	-2.3	0.27	-3.61	0.65	0.99	101 \pm 51 ¹	176	0.72 \pm 0.04	64
HD 149038	7.58	-2.8	0.18	-3.61	0.05	0.87	167 \pm 60 ¹	297	1.12 \pm 0.20	108
HD 149404	5.89	-3.0	0.37	-3.41	0.10	0.39	114 \pm 19 ¹	209	1.23 \pm 0.35	76
HD 149757	7.07	-2.8	0.14	-3.21	0.10	0.27	104 \pm 15 ¹	283	1.50 \pm 0.03	69
HD 151804	6.73	-2.9	0.45	-4.01	0.45	1.55	192 \pm 62 ¹	178	2.47 \pm 0.06	130
HD 152233	5.68	-3.0	0.14	-3.61	0.40	0.12	180 \pm 61 ¹	242	3.89 \pm 3.52	59
HD 152236	3.24	-3.0	0.24	-3.81	0.45	0.24	117 \pm 22 ¹	241	3.15 \pm 2.25	87
HD 152408	6.84	-2.9	0.49	-3.61	0.10	1.41	166 \pm 59 ¹	174	3.98 \pm 2.18	126
HD 154368	6.50	-3.1	0.31	-3.61	0.20	0.30	116 \pm 21 ¹	235	1.49 \pm 0.16	85
HD 164794	6.05	-2.5	0.16	-3.61	0.25	0.12	165 \pm 45 ¹	235	2.94 \pm 0.68	57
HD 193322	7.66	-2.7	0.14	-3.81	0.20	0.23	123 \pm 30 ¹	249	3.69 \pm 0.17	91
HD 199579	6.40	-3.1	0.25	-3.41	0.20	0.29	153 \pm 56 ¹	246	1.94 \pm 0.24	89
HD 203064	5.90	-3.0	0.26	-4.01	0.55	0.34	144 \pm 52 ¹	207	1.53 \pm 0.49	75
HD 206267	5.10	-3.1	0.20	-3.61	0.25	0.18	119 \pm 24 ¹	240	4.38 \pm 0.52	58
HD 209339	5.49	-2.4	0.08	-3.61	0.25	0.38	147 \pm 53 ¹	257	5.18 \pm 0.79	47
HD 209975	5.33	-2.9	0.18	-3.81	0.65	0.41	134 \pm 44 ¹	262	2.84 \pm 0.93	64
HD 210839	5.42	-3.0	0.12	-3.61	0.30	0.17	127 \pm 35 ¹	270	3.56 \pm 0.24	49
HD 303308	4.30	-2.9	0.12	-3.41	0.20	0.18	198 \pm 62 ¹	194	7.75 \pm 3.39	35
HD 027778 ³	4.76	-3.1	0.14	-3.0	0.10	0.83	93 \pm 32 ⁴	207	5 \pm 0.50	48
HD 037061 ³	4.47	-2.0	0.17	-2.4	0.05	1.05	99 \pm 36 ⁴	81	4 \pm 0.47	57
HD 116852 ³	4.86	-2.7	0.08	-3.4	0.15	1.54	116 \pm 102 ⁴	177	3 \pm 0.38	43
HD 122879 ³	6.44	-2.7	0.18	-3.4	0.10	6.19	365 \pm 94 ⁴	184	5 \pm 0.22	64
HD 147888 ³	3.34	-2.1	0.16	-3.5	0.20	2.28	98 \pm 23 ⁴	101	3 \pm 0.60	35
HD 185418 ³	5.05	-2.0	0.06	-3.7	0.30	4.14	173 \pm 34 ⁴	310	0.1 \pm 0.01	36

Table 2—Continued

Star	A_V/N_H (10^{-22} mag cm 2 H $^{-1}$)	α_S	$a_{c,S}$ (μ m)	α_C	$a_{c,C}$ (μ m)	χ^2/dof	[C/H] $_{\text{gas}}$ (ppm)	[C/H] $_{\text{dust}}$ (ppm)	[Si/H] $_{\text{gas}}^2$ (ppm)	[Si/H] $_{\text{dust}}$ (ppm)
HD 207198 ³	3.22	-2.8	0.06	-2.6	0.05	3.49	69 \pm 21 ⁴	168	3 \pm 1.34	21

¹ [C/H] $_{\text{gas}}$ estimated from n_H (see eq. 12).

² [Si/H] $_{\text{gas}}$ taken from Haris et al. (2016).

³ Model parameters taken from Mishra & Li (2015).

⁴ [C/H] $_{\text{gas}}$ taken from Parvathi et al. (2012).